Thermal fatigue as a driving mechanism for activity on asteroid Bennu

J. L. Molaro[1], C. W. Hergenrother[2], S. R. Chesley[3], K. J. Walsh[4], R. D. Hanna[5], C. W. Haberle[6], S. R. Schwartz[2], R.-L. Ballouz[2], W. F. Bottke[4], H. J. Campins[7], and D. S. Lauretta[2]

[1]Planetary Science Institute, Tucson, AZ, USA. [2]Lunar and Planetary Laboratory, University of Arizona, Tucson, AZ, USA. [3]Jet Propulsion Laboratory, Caltech Institute of Technology. [4]Southwest Research Institute, Boulder, CO, USA. [5]Jackson School of Geosciences, University of Texas, Austin, TX, USA. [6]School of Earth and Space Exploration, Arizona State University. [7]University of Central Florida, Orlando, FL, USA.

Key Points:

- We simulated stress fields in boulders to assess the nature and efficacy of thermal breakdown on Bennu, including by exfoliation.
- Our model predicts that exfoliation is capable of ejecting centimeter-scale particles from the asteroid at speeds of meters per second.
- This mechanism is consistent with observations of particle ejection at Bennu and is a viable explanation for Bennu's activity.

Abstract

Many boulders on (101955) Bennu, a near-Earth rubble pile asteroid, show signs of *in situ* disaggregation and exfoliation, indicating that thermal fatigue plays an important role in its landscape evolution. Observations of particle ejections from its surface also show it to be an active asteroid, though the driving mechanism of these events is yet to be determined. Exfoliation has been shown to mobilize disaggregated particles in terrestrial environments, suggesting that it may be capable of ejecting material from Bennu's surface. We investigate the nature of thermal fatigue on the asteroid, and the efficacy of fatigue-driven exfoliation as a mechanism for generating asteroid activity, by performing finite element modeling of stress fields induced in boulders from diurnal cycling. We develop a model to predict the spacing of exfoliation fractures, and the number and speed of particles that may be ejected during exfoliation events. We find that crack spacing ranges from ~1 mm to 10 cm and disaggregated particles have ejection speeds up to ~2 m/s. Exfoliation events are most likely to occur in the late afternoon. These predictions are consistent with observed ejection events at Bennu and indicate that thermal fatigue is a viable mechanism for driving asteroid activity. Crack propagation rates and ejection speeds are greatest at perihelion when the diurnal temperature variation is largest, suggesting that events should be more energetic and more frequent when closer to the Sun. Annual thermal stresses that arise in large boulders may influence the spacing of exfoliation cracks or frequency of ejection events.

Plain Language Summary

Soon after its rendezvous with the asteroid Bennu, the OSIRIS-REx spacecraft observed the asteroid to be ejecting tiny particles of material. Bennu is a rubble-pile asteroid covered in boulders of varying size. Many of these boulders show evidence of exfoliation, a process where thin layers of material are shed from their surfaces. Exfoliation is one consequence of thermal fatigue, which is the slow and progressive lengthening of cracks caused by the daily variation in boulder temperature from exposure to the Sun. Here we explore how thermal fatigue may cause the degradation and fracturing of boulders on Bennu and how the specific process of exfoliation could lead to the ejection of particles from the asteroid surface. We develop a model to predict the timing, number, and speeds of particles that may be ejected during exfoliation events, and compare our results to the spacecraft observations of the ejection events from Bennu's surface. Our results suggest that particles ejected from boulder surfaces during exfoliation can have speeds up to ~2 m/s and are most likely occur when Bennu is closest to the Sun and during the late afternoon, consistent with spacecraft observations.

1 Introduction

Observations of 101955 Bennu by the Origins, Spectral Interpretation, Resource Identification, and Security–Regolith Explorer (OSIRIS-REx) spacecraft have revealed a rough surface dominated by boulders with diverse morphologies and textures [*DellaGiustina and Emery et al.*, 2019; *Walsh et al.*, 2019; *Lauretta and DellaGiustina et al.,* 2019]. Signs of *in situ* bulk degradation, mass movement, craters, and visible fractures hint that its surface is influenced by a variety of weathering, impact, and other processes [*Barnouin et al.*, 2019; *DellaGiustina and Emery et al.*, 2019; *Walsh et al.*, 2019]. Although dedicated searches for asteroid activity during the spacecraft's approach detected none [*Hergenrother et al.,* 2019], navigational images taken from orbit have also unexpectedly revealed that Bennu has an active surface [*Lauretta and Hergenrother et al.*, 2019]. Multiple particle ejection events were observed starting in January 2019, shortly after the OSIRIS-REx spacecraft entered orbit, characterized as bursts of centimeter-scale and smaller particles leaving the asteroid surface. The two largest events occurred near asteroid perihelion, with numerous smaller events observed in the months following [*Lauretta and Hergenrother*, 2019; *Hergenrother et al., in review this collection*; *Leonard et al.*, in press*; Pelgrift et al.,* 2020]. Several mechanisms have been suggested to drive these ejection events, including electrostatic lofting of particles [*Hartzell*, *in review this collection]*, meteoroid impacts [*Bottke*, *in review this collection]*, phyllosilicate dehydration, and thermal fracturing [*Lauretta and Hergenrother*, 2019]. This work focuses on the lattermost mechanism, exploring its efficacy on Bennu's surface and possible contribution to ejection events.

Many of Bennu's boulders show signs of exfoliation, the flaking and disaggregation of thin layers of surface material. Recent work by Molaro et al. [2020] has demonstrated that these features on Bennu result from thermal fatigue, a subcritical crack growth process driven by diurnal thermal cycling [e.g., *Holzhausen*, 1989]. Previously, we lacked morphological evidence that fatigue could operate on airless body surfaces, though numerous studies had hypothesized that it may play an important role [e.g., *Dombard et al.*, 2010; *Jewitt and Li*, 2010; *Delbo et al.*, 2014]. Although models [*Molaro et al.*, 2015; *Hazeli et al.*, 2018; *El Mir et al.*, 2019] and laboratory investigations [*Thirumalai and Demou*, 1970; *Levi*, 1973; *Delbo et al.*, 2014] have provided valuable insight into its nature, the opportunity to study fatigue *in situ* on Bennu's surface provides new pathways for understanding how it drives landscape evolution and interacts with other surface processes such as micrometeoroid impacts. In terrestrial environments, fatigue often works in synergy with various chemical and biogenic weathering processes to drive boulder breakdown [*Waragai*, 1998; *McFadden et al.*, 2005; *Fletcher et al.*, 2006; *Eppes et al.*, 2010; *Eppes and Keanini*, 2017; *Lamp et al.,* 2017]. At very large scales, exfoliation of terrestrial rock domes is attributed to weakening of the rock via thermal fatigue, followed by critical failure due to compressive stresses from regional and/or seasonal thermal sources [*Martel*, 2011; *Collins and Stock*, 2016; *Martel*, 2017; *Collins et al., 2018; 2019*]. These spontaneous bursts of crack growth are observed to cause the release of audible acoustic waves and mobilization of particles off the dome surface [*Collins et al., 2018; 2019*]. Although the large scale of the stresses in these events are thought to add significant energy, this leads to the question of whether fatigue-driven, boulder-scale exfoliation may be capable of ejecting material from an asteroid surface, where less energy would be needed due to the microgravity environment. If so, this has important implications for our understanding of asteroid geology and the active asteroid population.

Here we investigate the nature of thermal fatigue on Bennu's surface and the efficacy of fatigue-driven exfoliation as a mechanism for generating asteroid activity. Following the description of the finite element model (Section 2), the paper has two primary focuses: (i)

describing boulder breakdown on Bennu and (ii) assessing its potential to cause asteroid activity (particle ejection). In Section 3, we perform modeling of stress fields induced in Bennu's boulders from diurnal thermal cycling to explore how thermal fatigue may drive the development of fractures and boulder morphologies observed on the asteroid surface. We compare our results to similar analyses done for terrestrial [*Eppes et al.*, 2016; *Lamp et al.,* 2017] and lunar [*Molaro et al.*, 2017] boulders, and studies that quantify scaling laws for estimating stress magnitudes and resurfacing rates on arbitrary asteroid surfaces [*El Mir et al.*, 2019; *Graves et al.,* 2019*; Ravaji et al.,* 2019], providing new insight into the efficacy of fatigue on carbonaceous chondrite materials and its expression on lunar versus asteroid surfaces. Section 3.2 describes the specific process of fatigue-driven exfoliation, which is then expanded upon in Sections 4 and 5 to explore how it may contribute to asteroid activity. In Section 4, we develop a model to predict the spacing of exfoliation fractures and the size and speed of particles that may be ejected from Bennu's surface during an exfoliation event, and in Section 5 we compare our results to observational constraints from Bennu's particle ejection events to assess the likelihood that thermal fatigue is their driving mechanism. All references to exfoliation in this text refer to exfoliation fully or partially driven by thermal fatigue, unless explicitly stated.

2 Finite Element Model

Following Molaro et al. [2020], we used COMSOL Multiphysics to perform finite element modeling of stress fields in three-dimensional spherical boulders on the surface of Bennu, with diameters ranging from 0.2 to 6 m. In each case, the boulder was embedded in unconsolidated regolith such that its lower half was buried. The regolith volume had sides which were fixed with respect to displacement and periodic with respect to temperature. The lower boundary had a net heat flux of zero and was fixed. The shared boundary between the regolith and boulder had a heat flux determined by the effective thermal conductivity of the two materials. This shared boundary, as well as the unburied boulder and regolith surfaces, were free to move in response to thermal forcing. Incident solar radiation was applied to unburied surfaces by adjusting the time-dependent solar position and distance computed using the NAIF (Navigation and Ancillary Information Facility) SPICE (spacecraft, planet, instrument, constants, and events) Toolkit. The coordinates were computed at an equatorial location over one solar day at Bennu's perihelion. The model takes into account the local surface slope and orientation of individual mesh elements, scattered and exchanged radiation from surrounding elements, and the size of the solar disc during a local sunrise or sunset.

The boulders were assumed to have the bulk properties of terrestrial serpentinite (Table 1), as the closest spectral matches to Bennu's surface are aqueously altered CM carbonaceous chondrites [*Hamilton et al.*, 2019], which are composed primarily of serpentine-group phyllosilicates [*Howard et al.,* 2009]. We simulated both "dense" and "porous" boulders, with properties representing each end of serpentinite's range of porosities (10 to 35%, respectively). This porosity range may represent compositional or structural differences in the rock due to its formation, or due to subsequent accumulation of damage. The properties associated with the porous boulders are comparable to measurements of the thermophysical properties of CM chondrites and other possible Bennu analogs [*Opeil et al.*, 2010; *Macke et al.*, 2011; *Horai*, 2012]. The difference in stress magnitude observed between dense and porous simulations is due primarily to the change in Young's modulus as a result of increased porosity, as the thermophysical properties have only a weak (up to a few percent) influence on the results [*Molaro et al.*, 2017].

The thermophysical properties of the regolith were determined by ensuring that the effective thermal inertia of the combined regolith and boulder surfaces matches that of Bennu (350 J/m^2 K s^{½}) [*DellaGiustina and Emery et al.*, 2019], and therefore that it realistically approximates the asteroid's thermal environment. The regolith was assumed to have mechanical properties comparable to lunar regolith such that it did not impose any confining pressure on the boulders.

We then calculated the heat equation for heat transfer in solids in order to calculate the temperature and stress fields within the boulders over time. A full description of the equations solved by COMSOL for this calculation, as well as an expanded discussion of the model details, justification for the material properties in Table 1, and information on model uncertainties can be found in Molaro et al. [2020] and in Supporting Information Text–1. A discussion of the influence of boulder shape and surface roughness on our results is included in Section 3.4 and Appendix A.

Table 1. Thermal and mechanical properties of simulated materials.

Property	Units	Dense [a] Boulders	Porous [b] Boulders	Regolith [c]	References
Density (ρ)	kg/m^3	2510	1812	1190	[a][*Christensen*, 1966], [c][*Vasavada et al.*, 2012]
Thermal Conductivity (k)	W/m K	2.5	0.5	[a]0.076, [b]0.125	[a,b][*Horai*, 2012], [b][*Opeil et al.*, 2010], [c][*Vasavada et al.*, 2012]
Heat Capacity (c_p)	J/ kg K	$c_p(T)$	$c_p(T)$	$c_p(T)$	[*Ledlow et al.*, 1992]
Albedo (A)		0.044	0.044	0.044	[*DellaGiustina and Emery et al.*, 2019]
Young's Modulus (E)	GPa	35	15	8 x 10^{-3}	[a][*Christensen*, 1966], [b][*Burk*, 1964], [c][*Colwell et al.*, 2007]
Poisson's Ratio (ν)		0.34	0.05	0.4	[a][*Christensen*, 1966], [b][*Burk*, 1964], [c][Colwell et al., 2007]
Coefficient of Expansion (α)	1/K	8 x 10^{-6}	8 x 10^{-6}	2.4 x 10^{-4}	[a, b][*McKinstry*, 1965], [c][*Agar et al.*, 2006]

3 Model Results and Discussion

Before we can assess the contribution that thermal breakdown makes to asteroid activity, we use our simulations to examine its general nature on Bennu's surface. The magnitude of stress fields experienced by the boulders can be used to determine whether the threshold for crack propagation is met. The model does not simulate crack propagation itself, but the orientation of the stress fields informs where and when microcrack propagation tends to occur. The stress fields induced in boulders undergoing thermal cycling are spatially and temporally complex. Tensile stresses arise in different parts of the boulders at different times of day, and their orientation leads to crack propagation in different directions. Although all of these stresses are part of the boulder's continuous mechanical response to heating, it is helpful to think about certain effects as separate stress fields that each contribute differently to the overall morphological evolution of boulder shapes and sizes over time. Molaro et al. [2017] illustrated the three primary stress fields (Figure 1) induced by diurnal cycling in lunar boulders: deep interior stresses that drive through-going fractures, near-surface stresses that drive surface-parallel fractures ("exfoliation"), and surface

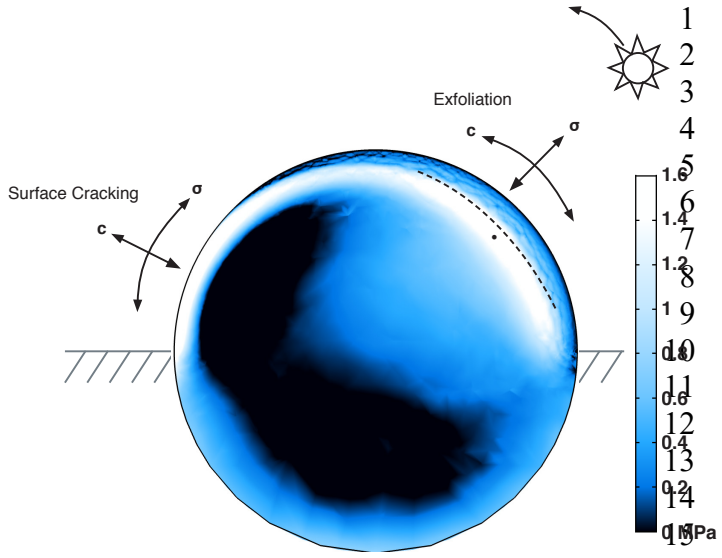

Figure 1. Stress field in a cross section of a 2 m boulder at mid-morning, showing developing exfoliation stresses on the boulder's east face and surface cracking stresses on its west face. Lines show the direction of stress (σ) and cracking (c). The dashed line shows the approximate exfoliation depth, and the dot is the approximate location maximum of the exfoliation stress field. The Sun moves from right to left in the plane of the image. Regions that are black have negative (compressional) stress.

stresses that drive shallow surface-perpendicular fractures ("surface cracking"). We discuss each of these effects in the context of observations of Bennu's boulders. Parameters from the simulations will also feed into the crack spacing and particle ejection model discussed in Section 4, which we relate to the observed particle ejection events at Bennu [*Lauretta and Hergenrother et al.*, 2019; *Leonard et al.*, *in press*]. We examine only boulder-scale effects in this work, but stresses induced at the mineral grain scale could also play a role in the distribution of microcracks that develop into larger-scale features [e.g., *Molaro et al.,* 2015; *Hazeli et al.,* 2018].

3.1 Stress Magnitudes

To determine whether thermal fracturing may occur, we can quantify the magnitude of thermally induced stress in boulders, which is controlled by the amplitude of temperature variation they experience and their thermophysical and mechanical properties. Stresses are highest in dense, brittle materials that do not easily deform in response to thermal forcing, and each stress field varies differently with boulder size (Figure 2). Stresses in boulders that are more porous are weaker in magnitude, though their orientations remain unchanged. Surface stresses range from ~2 to 5 MPa, increasing with boulder diameter as a result of decreased surface curvature. Exfoliation and deep interior stresses are controlled by the size of the boulder with respect to the diurnal skin depth. They peak at a diameter of ~5× the skin depth and decrease in larger boulders, ranging from ~0.4 to 3 MPa and ~0.2 to 2 MPa for exfoliation and interior stresses, respectively. These are comparable to the tensile strengths of our terrestrial serpentinite analog (0.5 to 5 MPa) [*Burk*, 1964; *Altindag et al.*, 2010] and similar soft, anisotropic materials such as limestone and shale (1 to 12 MPa) [*Sanio*, 1985; *Chen et al.*, 1998]. Even the weakest stresses are comparable to the estimated tensile strength of boulders on (162173) Ryugu (0.2 MPa) [*Grott et al.*, 2019], which is also a carbonaceous asteroid. Such conditions make it plausible for thermal fracture processes to be active at Bennu.

The most likely thermal fracture process to occur is fatigue, which, as a subcritical crack growth process, requires a stress lower than the material's ultimate tensile strength in order to

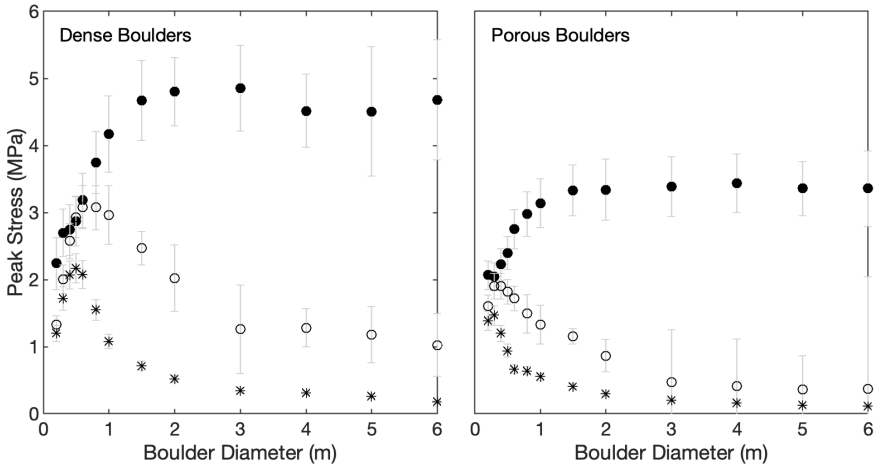

Figure 2. Peak surface (solid circle), exfoliating (open circle), and deep interior (asterisks) stresses in dense (left) and porous (right) boulders of varying diameter. The error bars represent uncertainty due to mesh size and location of peak stress (see Supporting Information Text–1 and Molaro et al. [2020] for full details).

propagate cracks. Crack propagation models typically describe stress fields in terms of the stress intensity factor, a term that relates the stress around the tip of a crack to the macroscopic stress field [*Lawn,* 1993]. In terrestrial environments, the threshold to drive sub-critical crack growth requires a stress intensity factor that is ~10 to 20% of the material's fracture toughness [*Atkinson,* 1984]. To first order, surface-parallel microcracks can be approximated as cracks in an infinite medium, where the material's fracture toughness is linearly proportional to its tensile strength [*Emmerich,* 2007]. Our results (Figure 2) show we have sufficient stress to overcome a threshold of 20% of the tensile strength, indicating that fatigue is likely to be active at Bennu. Observations of boulder morphologies on the surface are consistent with fatigue-driven exfoliation [*Molaro et al.*, 2020]. On Earth, however, fatigue is typically aided by stress corrosion and other synergistic chemical weathering mechanisms [*Fletcher et al.*, 2006; *Aldred et al.*, 2016; *Eppes and Keanini*, 2017; *Lamp et al.* 2017], and studies have shown that crack propagation in vacuum can be harder to achieve [*Krokosky and Husak*, 1968; *Thirumalai and Demou*, 1970; *Kranz*, 1979]. This makes it unclear what threshold is needed to drive fatigue in asteroid environments, though better constraints on material strengths and fatigue thresholds will be enabled by analysis of the samples that OSIRIS-REx will return to Earth.

If Bennu's materials are sufficiently weak, it is plausible that thermal shock processes [*Walsh and Lomov,* 2013; *Browning et al.,* 2016; *Thirumalai and Demou*, 1970; *Richter and Simmons*, 1974], which occur when an object's tensile strength is exceeded, could also drive crack propagation on Bennu. Such processes could have occurred during Bennu's migration to near-Earth space as its surface materials normalized to a warmer thermal environment. However, the prevalence of boulders on the asteroid surface and the relative lack of finer material [*DellaGiustina and Emery et al.,* 2019; Lauretta and DellaGiustina et al. 2019; *Walsh et al.,* 2019] are not consistent with the rapid erosion rates associated with shock processes [*Kendrick et al.,* 2016; *Wang et al.,* 2016; *Atkinson,* 1984], which would break down boulders quickly oven over Bennu's shortest predicted migration period [100 Myr; *Walsh et al.,* 2019]. Any shock processes that occur today are likely limited to freshly exposed boulders faces, e.g., by mass movement or

impacts [*Walsh et al.,* 2019]. Thus, we focus the remainder of our discussion on thermal fatigue, which we interpret to be a much more likely driver of rock breakdown on Bennu. The way in which subcritical growth via fatigue can lead to critical failure and energetic particle ejection is discussed in Sections 3.2 and 4.

The magnitude of diurnal stresses decreases with increasing solar distance (for a body with a given rotation rate) due to the reduction in insolation. Because fatigue crack propagation rates have a nonlinear relationship to stress [e.g., *Lawn,* 1993], this will cause variation in fatigue efficacy throughout the orbit, which adds complexity to estimating fracture development timescales using models [e.g., *El Mir et al.,* 2019]. For a 1-m boulder on Bennu, the variation in stress with solar distance (s) is approximately proportional to $s^{-1.2}$, which is consistent with previous models and scaling laws [*Ravaji et al,* 2019; *Molaro et al.,* 2017]. For flat ground, a similar decrease in stress magnitude would occur with increasing latitude. However, due to its large-scale surface roughness, high (relative) diurnal temperature amplitudes occur at all latitudes on Bennu [Rozitis et al., 2020*J*. This suggests that fatigue does not necessarily occur more slowly at high latitudes, though it likely affects a smaller part of the boulder population. An overall decrease in fatigue efficacy with latitude would be more likely on an asteroid whose boulders are smaller in scale relative to the body's surface curvature. Compared to the equatorial boulders, the orientation of stress fields in boulders at non-equatorial latitudes is rotated relative to the direction of the Sun's path (Section 3.4 and Appendix A).

Overall, these stresses have lower absolute magnitudes than those reported by Molaro et al. [2017] for lunar boulders because the diurnal temperature variation on Bennu is smaller and the boulders have a lower Young's modulus. However, stresses in lunar boulders are an order of magnitude lower than their presumed tensile strength, and the lunar cycling rate is only 12 cycles/year compared to Bennu's 10^3 cycles/year. Combined, these two factors suggest that thermal fatigue on the Moon happens more slowly than on Bennu. Recent works examining lunar boulder populations suggest that thermal fatigue is relevant in meter-scale boulders [Li et al., 2017], but overall is subordinate to impact processes in driving breakdown [*Basilevsky et al.*, 2015; *Ruesch et al.,* 2020]. There are currently no constraints on the relative rates of weathering by impacts and fatigue on Bennu. One notable difference between the two bodies is that lunar boulders ~8× the diurnal thermal skin depth (4 to 7 m) show a local maximum in the trend of stress with diameter [*Molaro et al.,* 2017; their figure 10], which is distinct from where the peak exfoliation stress occurs (~11× the skin depth, ~9 m). Boulders near this local maximum are predicted to break down most efficiently from thermal fatigue due to the strong heat flux emitted from their surfaces near sunset, in concert with the boulder size relative to the thermal skin depth. This effect is not present on Bennu because of its smaller temperature range, and instead stresses are dominated by boulder size and temperature gradients. Bennu's peak exfoliation stress also happens at a smaller relative boulder size (~5× its skin depth) than on the Moon. These factors highlight that the boulder population will evolve differently on different bodies as a result of thermal effects.

3.2 Exfoliation

Near-surface stresses lead to boulder exfoliation, which is observed widely at Bennu and likely to be driven by thermal fatigue [*Molaro et al.,* 2020]. It is relevant to review how fatigue-driven exfoliation operates here because it is this mechanism which we propose leads to the observed

ejection of particles from Bennu's surface. This discussion directly informs the crack spacing and particle ejection calculations performed in Section 4.

Exfoliation is driven by thermally induced stresses that arise in boulder near-surfaces during daytime heating [e.g., *Holzhausen,* 1989; *Martel,* 2011; *Molaro et al.,* 2017], as illustrated in Figure 1, which shows the stress field on a cross section through a boulder at mid-morning. The boulder surface moves into a state of compression as it heats, causing a region of tension to develop in the near-surface associated with the spatial temperature gradient. As the Sun moves overhead, this tensile region expands westward and the location of its local maximum follows along a plane parallel to the boulder's surface. These "exfoliation stresses" have a surface-normal orientation, pointing approximately in the Sun's direction and driving microcrack propagation along surface-parallel planes. Over time, larger-scale fractures can develop as microcracks coalesce [*Jansen et al.,* 1993], leading to the development of an exfoliation flake that separates from the boulder surface. Once it has begun to disaggregate, expansion and contraction of the flake itself can aid in lengthening the underlying crack [*Collins and Stock,* 2016; *Lamp et al.,* 2017]. The rate at which crack propagation occurs increases as its length grows relative to the boulder size, and when it nears a boundary (e.g., boulder edge or material discontinuity) will transition abruptly from sub-critical to critical failure [e.g., *Janssen et al.,* 2002]. This instantaneous, catastrophic disruption at the end of a fatigue crack's life can cause disaggregation of all or part of the flake, and in terrestrial environments has been observed to result in rockfalls and mobilization of particles off the surface [*Collins and Stock,* 2016; *Collins et al., 2018; 2019*]. It is this mechanism which we hypothesize to cause ejection of particles from Bennu's surface. In Section 4, we will quantify the available energy in these events that can go towards ejecting particles such events and estimate the particular sizes and speeds.

Terrestrial observations show that one or more surface-parallel fractures may develop within the exfoliation region [e.g., *Martel*, 2017], the spacing of which controls the thickness of layers that disaggregate from the surface. In three dimensions, the exfoliation stress field is shaped somewhat like a spherical cap, and as a result the depth to which the stress orientation is surface-normal (the "exfoliation depth") is shallower than the depth of the local stress maximum at the center (Figure 1). The exfoliation depth varies over time and is not symmetrical with respect to the local subsolar point at the boulder surface. It typically falls between ~1 and 3 diurnal thermal skin depths, and may reach deeper in some parts of the boulder due to interaction with other stress fields. This variation makes it difficult to quantify the exfoliation stress consistently across boulder sizes and at different times of day, so it is useful to use the stress magnitude at the local maximum as an upper limit. This magnitude, which is controlled by both the boulder size and the diurnal thermal skin depth, is reported as the maximum exfoliation stress in Figure 2. The magnitude of stress at the exfoliation depth is typically 50–80% of that at the local maximum and decreases towards the boulder surface until entering the compressive regime (negative stress). Surface parallel fractures may develop at any point shallower than the exfoliation depth where the stress and energy requirements to drive crack propagation are met (Section 4).

3.3 Other Expressions of Fatigue

While exfoliation is the most relevant process pertaining to asteroid activity (Section 4), stress fields elsewhere in boulders may produce other breakdown behaviors on Bennu. The highest thermal stresses that occur in boulders undergoing thermal cycling are at their surfaces during surface cooling at night. These are limited in depth to the upper thermal skin depth and drive

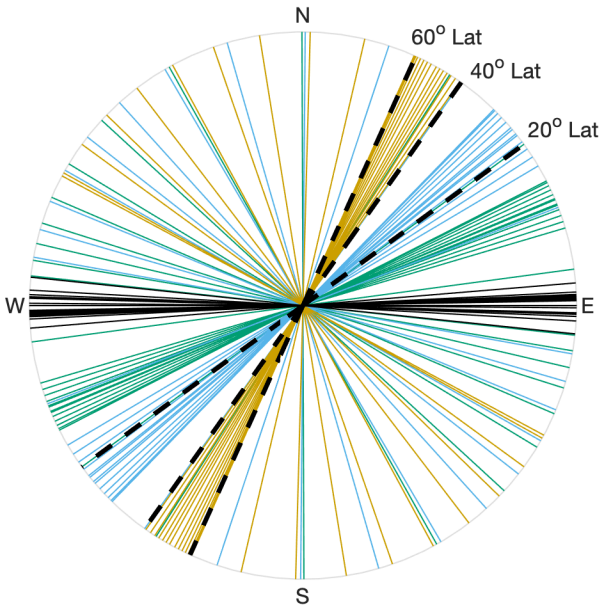

Figure 3. Orientation of stress at the center of a 1 m boulder at the equator (black), 20 degrees latitude (green), 40 degrees latitude (blue), and 60 degrees latitude (orange) on Bennu at solar hour intervals. The black dashed lines show the orientation at the time of peak stress for each boulder above the equator.

18

surface-normal crack propagation ("surface cracking") that is expected to contribute to shallow effects such as surface disaggregation or granular disintegration. Many boulders on Bennu appear to be breaking down in ways consistent with surface cracking, featuring loose particles seemingly disaggregated from their surfaces, surrounded by unresolved material, or containing cracks that follow apparent clast boundaries [*DellaGiustina and Emery et al.*, 2019; *Walsh et al.*, 2019; *Molaro et al.,* 2020]. Surface cracks are likely to be the dominant mechanism serving to break up exfoliation flakes into smaller particles as they disaggregate. Even if they do not cause disaggregation directly, any damage accumulated in the form of microcracks at the boulder surface can weaken flakes, enabling pieces to break off during exfoliation events, or making them more susceptible to breakup from impacts. Damage accumulation in the upper few thermal skin depths may also increase the porosity of boulder surfaces relative to their less damaged interiors. This will make it more challenging to constrain the thermal and mechanical properties of Bennu's bulk materials from both spacecraft data and returned samples, which has important implications for impact modeling and other research focused on understanding the formation and evolution of rubble-pile asteroids. Different materials are more or less susceptible to different types of damage accumulation depending on their mineral composition and fabric, and therefore studying variation in surface thermal inertia with respect to the boulder population may provide important insight.

Another expression of thermal fatigue that may be visible on Bennu is the presence of linear, through-going fractures that are inferred to result from stresses occurring in the deep interior of boulders [*Molaro et al.*, 2017]. These stress fields produce a predominant N-S trend in fracture orientation, which has been identified in boulder populations on Earth [*McFadden et al.*, 2005; *Eppes et al.*, 2010], Mars [*Eppes et al.*, 2015], and the Moon [*Ruesch et al.,* 2020]. Figure 3 (black solid lines) shows the stress orientation at solar hour intervals throughout the day at the center of a 1-m boulder at Bennu's equator. These remain approximately in the E-W plane, which tend to drive crack propagation in the N-S direction at boulder interiors. Microcracks can coalesce into large-scale features that reach the boulder edges, and may become through-going fractures that split boulders apart. McFadden et al. [2005] inferred from observations that the predominant fracture orientation should vary with latitude as the position of the boulder changes relative to the

Sun. This is supported by our results, which shows the stress field shift from an E-W to NE-SW orientation with increasing latitude (Figure 3 left; green, blue, orange). The orientation of the stress field at the time of peak magnitude has an aspect angle (degrees east of north) of 54, 35, and 25 degrees for boulders at 20, 40, and 60 degrees latitude, respectively. This orientation never becomes truly N-S at the highest latitudes, as it will always be influenced by the position of the Sun and the E-W direction of its motion. This suggests that the trend in predominant fracture orientations should shift from N-S near the equator towards NW-SE and NE-SW at higher and lower latitudes, respectively. Statistical mapping of the orientation of through-going fractures observed on Bennu [*Walsh et al.*, 2019; *Molaro et al.,* 2020] is needed to assess whether this trend is present, though it may be influenced by mass movement [*Walsh et al.*, 2019; *Barnouin et al.,* 2019; *Jawin et al.* submitted]. Such work may provide additional constraints on fatigue stress thresholds and crack propagation rates for carbonaceous chondrite materials.

3.4 Influence and Evolution of Boulder Shapes

Expressions of thermal fatigue on Bennu may be influenced by realistic boulder shapes, as variation in the amount and timing of incident solar radiation on their surfaces may change where and how efficiently different fatigue-driven features develop due to face orientation and surface/shape roughness. Boulders that are very angular and/or have highly sloped faces may experience considerable changes in heating throughout the day, depending on their orientation with respect to the Sun. For example, a highly sloped east-facing surface heats quickly at sunrise but also becomes self-shadowed early in the day. As a result, it experiences a reduction in diurnal temperature variation relative to another face and lower surface stresses may lead to less surface cracking. An increase in local surface curvature due to surface roughness can have a similar effect. On very angular boulders, faces that are oriented away from the Sun may receive little incident radiation. Such an effect could serve to reinforce or retain the boulder's angular shape by only causing degradation of the sunward-facing surfaces. Exfoliation may smooth or reinforce a boulder's shape depending on the scale of surface or shape roughness relative to the thermal skin depth. Fractures may develop underneath small-scale bumps and cracks on boulders, leaving a smoother surface behind after a flake disaggregates. As the roughness of the shape approaches the scale of a few thermal skin depths, different portions of the boulder may begin to behave like separate or disparate segments, with exfoliation occurring independently on each. See Appendix A for additional discussion on such effects.

Stress fields driving different fractures also interact differently in boulders of different size. There is a synergy between interior and exfoliation stresses in boulders ≤ 1 m, for which the diurnal thermal skin depth is a significant fraction of their size. In these cases, exfoliation stresses on the E and W sides of the boulder are aligned and overlap with the deep interior stress field. This may result in the more efficient development of through-going fractures at the expense of exfoliation and/or in the deepening of exfoliation cracks, causing the distinction between the two features to blur. Thermal fatigue is likely to have a strong interaction with the variety of rock fabrics and textures observed on Bennu [*Molaro et al.*, 2020], and the presence of layering effects in some boulders, particularly those ≤ 1 m in size, may cause the deviation of exfoliation cracks from surface parallel to linear paths. As boulders become larger growing to sizes ≥ 3 m, their western and eastern edges become more mechanically decoupled. It takes longer for the nighttime surface stresses on their western edges to dissipate and the region to become dominated by the daytime stress field as it overtakes the eastern hemisphere. Additionally, western surface stresses

have much greater magnitudes than in smaller boulders. This results in large boulders retaining very strong stresses at their western surfaces and near-surfaces throughout the day that could perhaps lead to asymmetrical breakdown of boulders.

3.5 Annual Stresses

Bennu experiences an annual thermal cycle that may also drive thermal fatigue and/or influence the rate and location of crack propagation caused by diurnal effects. This annual thermal cycle results from the asteroid's eccentric orbit, which causes its solar distance to vary between 0.89 and 1.36 au throughout its 436.7 Earth-day year and resulting in an annual variation in surface heating. The annual thermal skin depth is ~5.6 and 2.9 m for dense and porous boulders, respectively, allowing annual stresses to penetrate much deeper than the diurnal effects that dominate their surfaces. Annual effects start to become important in boulders with diameters >3 m (though their effects are not included in our diurnal simulations above), in which stress fields analogous to the exfoliation and interior stresses described above arise at different times of year.

Annual stresses are challenging to model because spatially resolving both annual and diurnal scales in the simulation requires extremely large mesh sizes and is very computationally expensive. Using the same method described above, we simulated a 10 m equatorial boulder over an entire Bennu orbit with the highest possible mesh resolution given the restrictions on computation times. This resolution is still lower than acceptable for the diurnal simulations, and therefore there is high uncertainty in the resulting magnitude of induced stresses. The stresses at the boulder center and its near-surface, measured below the depth that diurnal surface stresses reach, are on the order of 1 MPa and peak during perihelion approach. These are likely an overestimate of actual annual stresses; however, given the order of magnitude agreement with diurnal stress magnitudes, it is likely that that annual stresses are still great enough to overcome the subcritical threshold needed to drive thermal fatigue.

In spite of the uncertainty in magnitude, the orientations of annual stresses can provide insight into how they may influence rock breakdown. In the near surface, the stress orientation is surface perpendicular during perihelion approach. This is caused by net heating of the boulder as the asteroid moves closer to the sun, setting up a temperature gradient and stress field analogous to diurnal exfoliation effects. On perihelion departure, net cooling is most efficient out of the N and S faces of the boulder, which drives fractures in the E-W plane. At the boulder center, the stress orientation alternates between E-W during perihelion approach and the z direction (surface-normal) during departure, which is the same pattern as the diurnal stresses that drive N-S through-going fractures. This suggests that if annual stresses are strong enough to drive fatigue, such fractures should be seen at both spatial scales and should develop most efficiently in boulders subject to both diurnal and annual cycles, where their effects reinforce each other. A better understanding of their relative rates is needed to assess how annual stresses may disaggregate large boulders and the implications for the evolution of the boulder size-frequency distribution. In the near surface especially, it is unclear to what depth diurnal effects may operate quickly enough to dominate breakdown and whether annual fractures may be exposed by such disaggregation. Further, very large boulders are likely to have substantial preexisting damage and structural inhomogeneities that fatigue will exploit. These factors may make it difficult to identify annually driven features on Bennu's surface, though boulder size may be one distinguishing constraint.

The magnitude of annual stress in boulders is greatest when oriented in such a way as to drive an annual exfoliation effect in the near surface, suggesting that terrestrial sheeting joints may

be a relevant analog to observations. On Earth, the development of large-scale sheeting joints is commonly attributed to regional compressional stresses that result in surface-normal tensile stress in the near surface [e.g., *Martel,* 2011; *Martel,* 2017]. Joints occur as many surface-parallel cracks with characteristic spacing that is thin near the surface and increases with depth. They are similar to diurnal exfoliation layers but occurring at larger scales, with layers ranging from millimeters to tens of meters thick [*Martel*, 2017]. Regional tectonic stresses are not expected in a microgravity environment, but annual stresses on asteroids could play an analogous role, driving the development of surface-parallel fractures at depths below where diurnal effects operate. Further, diurnal and seasonal thermal stresses are known to contribute to sheeting joint exfoliation [*Collins and Stock,* 2016; *Collins et al., 2018; 2019*], suggesting that the superposition of annual and diurnal stress fields and/or sets of fractures in Bennu's boulders may influence the rate and/or location of diurnally driven crack propagation. These factors highlight the complexity of understanding how such features develop on asteroid surfaces and may help to explain the observation of some exfoliation layers on Bennu that are thicker than typical diurnal exfoliation depths [*Molaro et al.*, 2020].

3.6 Influence of Volatiles

Although volatiles from pore ice are not expected [*Rozitis et al.*, 2020], Bennu's surface is dominated by hydrated phyllosilicate minerals [*Hamilton et al.*, 2019], which may lead to synergies with thermal fatigue [*Lauretta and Hergenrother et al.* 2019]. CM carbonaceous chondrites are largely composed of serpentine-group phyllosilicates that contain tightly bound hydroxyl ions within octahedral sheets. Dehydroxylation can result from heating, comminution, and space weathering [*Drief and Nieto*, 1999; *Nakamura*, 2005; *Lantz et al.*, 2015; *Thompson et al.*, 2019], resulting in both pore space and molecular water. The former is caused by the volume change associated with the dehydration reaction and may result in cracks that weaken the bulk material and enable water migration (Tenthorey and Cox, 2003). The absorption of the water molecules onto crack walls can lower their surface energy and therefore the critical stress threshold required to drive crack growth [*Krokosky and Husak*, 1968; *Thirumalai and Demou*, 1970; *Kranz*, 1979], which may enhance and accelerate the fatigue process. Indeed, laboratory studies have shown that hydrated carbonaceous chondrite meteorites develop cracks under thermal cycling more quickly than anhydrous ordinary chondrites [*Delbo et al.*, 2014]. If present, these effects may be analogous to the environmentally assisted crack propagation (stress corrosion) that is thought to facilitate or enhance fatigue in terrestrial environments [*Aldred et al.*, 2016; *Eppes and Keanini*, 2017; *Lamp et al.,* 2017]. However, the intrinsic source of water in these materials has important implications for how boulders break down relative to terrestrial observations. If thermal dehydroxylation occurs in Bennu's boulders, it cannot be physically decoupled from the mechanical stresses that are induced by thermal forcing, and therefore any effects from the process would be intrinsically captured in the material's effective strength and Young's modulus. In this context, the properties of asteroid materials not only depend on their composition, but also their temperature and age. This suggests that the efficacy of thermal fracturing processes may vary widely between asteroids and asteroid populations, as well as throughout their orbital and geomorphological histories. These effects are not directly included in our simulations but would be reflected in the range of density and Young's modulus values of the boulders, which currently are not known for Bennu.

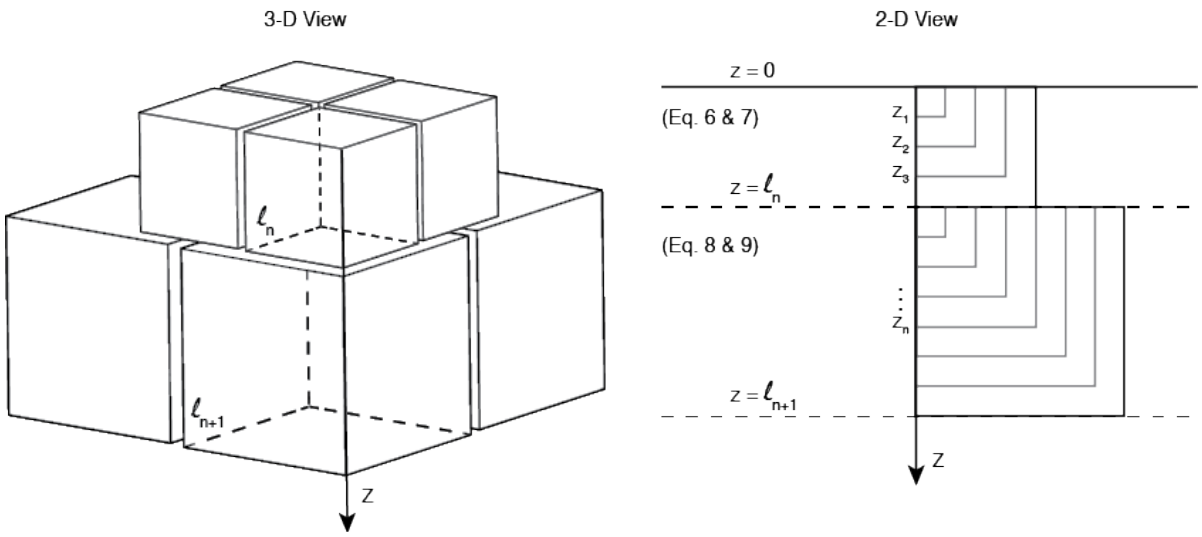

Figure 4. (left) Three-dimensional and (right) two-dimensional views of the layer geometry assumed in our crack spacing and particle ejection calculations.

4 Crack Spacing and Particle Ejection

We hypothesize that fatigue-driven exfoliation is the mechanism responsible for driving the ejection of particles from Bennu's surface — specifically, at the transition from sub-critical to critical crack growth, where the catastrophic failure of the separating flake produces mobilized fragments of rock (Section 3.2) [*Janssen et al.,* 2002; *Collins and Stock,* 2016; *Collins et al., 2018; 2019*]. We can test this hypothesis by comparing the characteristic spacing of exfoliation layers, which determines the sizes of particles disaggregated from the boulder, to the observed particle population. We can also use the predicted energy associated with these critical events to estimate particle ejection speeds.

A necessary condition for crack growth to occur, whether critical or subcritical, is the presence of enough energy to create the new crack walls. We use the thermal strain energy density within our simulated boulders to create a model (Figure 4) to predict the spacing of surface-parallel exfoliation cracks (Figure 5) that may develop [e.g., *Fletcher et al.*, 2006]. The thermal strain energy is potential energy stored within an object as it undergoes elastic deformation in response to a change in temperature. If there is sufficient stress in an object to drive crack propagation, strain energy is released as the crack grows, providing the energy that goes into producing its new crack walls. As with our previous analysis (Section 3), we do not model actual crack growth within the boulders, but we do quantify the characteristic spacing of exfoliation cracks by determining where enough energy is available to create them. For boulders undergoing diurnal cycling, this energy is generated, stored, and then dissipated in the boulder throughout each cycle, each day providing energy for progressive crack lengthening. The strain energy is highest in the late afternoon (Figure 6) when they have undergone the most expansion due to surface heating. This is the same time at which the exfoliation stress is highest (and therefore exfoliation events are most likely) and represents the most amount of energy available to propagate surface-parallel cracks during the day. As a result, exfoliation events are of the most interest with respect to producing particle ejection, though we also consider events produced by surface cracking.

We assume that a fracture will form where the accumulated strain energy with depth is equal to the surface energy of the new crack walls that will be created as a result. Our simulations are three-dimensional so the strain energy density in the boulder is not spatially uniform in any dimension. We take a linear profile of the strain energy density from the boulder's center to its surface at the time and (surface) location where the peak value occurs. This we use as the depth-dependent energy density of the boulder, making the simplifying assumption that it is uniform along the surface-parallel plane. This assumption holds true for a region approximately half a hemisphere around the location of peak strain energy. (These energy density profiles are included with the data available in the repository noted in the acknowledgements.) We then calculate the depth (l) at which a fracture will form, disaggregating the layer of material above it. We assume that this layer fragments into many equally sized blocks with the dimension of the fracture depth (Figure 4). The energy an individual block needs to contain for this to occur is:

$$E_n = 6\gamma l^2 \quad (5)$$

where γ is the surface energy of the rock. Enough energy is needed to create six crack walls: four vertical boundaries, one lower boundary, and the upper boundary of the layer below (Figure 4). To determine the energy available (E_a) in the boulder, we integrate the strain energy density (U) with depth to obtain:

$$E_z = \int_{z=0}^{z'} U(z)dz \quad (6)$$

and multiply it by the surface area in the other two dimensions, giving a total available energy:

$$E_a = E_z z^2 \quad (7)$$

A fracture is assumed to form at the depth (l) at which the energy available in the block is equal to the energy required ($E_a = E_n$), found using Eqs. (5) and (7). Once the depth of a given fracture (l_n) is determined, the value of E_a is reset to zero and can begin accumulating once more such that for $z > l_n$:

$$E_{z>l} = \int_{z=l_{n-1}}^{l_n} U(z)dz \quad (8)$$

and:

$$E_a = E_z(z - l_n)^2 \quad (9)$$

We could instead assume that a layer disaggregates as a cohesive, disc-shaped fragment, but subsequent investigation into possible particle ejection speeds would require invoking an additional energy source to then fragment the disc into smaller pieces. Although portions of flakes may disaggregate cohesively, it is reasonable to assume that factors such as surface stresses at different times of day and other mechanisms such as micrometeoroid impacts [*Bottke et al., in review this collection*] will contribute to the breakup of flakes into smaller particles as they develop. By choosing to incorporate the energy requirement for breaking up the flake into this calculation, this method provides a more conservative estimate of the number of surface-parallel

fractures that can form as a result of exfoliating stresses and an upper bound on the largest expected layer thickness. Any particles deposited atop boulders from other processes can still be mobilized when an exfoliation flake experiences a lengthening event, but their numbers cannot be constrained by this model.

The number of particles (N) into which each layer fragments can be calculated by taking the volume of a spherical cap of height l_n, subtracting the layer above, and dividing it by the volume of an individual cubic particle:

$$N = \frac{\pi}{3(l_n - l_{n-1})^3}\left[l_n^2(3R - l_n) - l_{n-1}^2(3R - l_{n-1})\right] \quad (10)$$

where R is the boulder radius. This method provides a more conservative estimate than dividing the flat area of the spherical cap by l_n^2, but it is ultimately an upper bound on the number of particles into which flakes may fragment.

The previous calculation makes the assumption that a crack will form where there is enough available strain energy. However, several factors may influence realistic crack depths and can change the amount of available energy in a given exfoliation layer. Exfoliation layers form progressively, and there must still be sufficient stress to drive crack growth at any given location. Because stresses are weakest near the surface, the fatigue threshold to develop a crack may be achieved at a greater depth than the required strain energy. At depths where the fatigue threshold is met, thin layers may also develop more slowly due to lower stresses than layers at depth. Any layer that disaggregates contains all available strain energy within its volume, including that which Eqs. (5) to (9) assume goes into the development of shallower layers. Therefore, if those shallower cracks are not propagating at the same rate as a deep crack, excess energy may be available beyond what is needed to form the disaggregating layer. Other factors can also contribute to this. For example, partially formed exfoliation flakes may become closer to the surface as material is disaggregated, altering the depth where it is energetically favorable to propagate cracks and requiring less energy to disaggregate new material. Structural weaknesses or pre-existing damage in boulders could have similar effects. In any of these cases, excess energy may be available within disaggregated particles that can go towards ejection.

If we prescribe that a single crack forms at some arbitrary depth, we can calculate the amount of excess energy (E_e) available within particles using the same geometrical assumptions as in Figure 4. In this case, none of the strain energy in the boulder goes into disaggregating layers above that depth, so we use Eqs. (5) and (9) to find:

$$E_e = E_a - E_n \quad (11)$$

This is converted to kinetic energy, ignoring the effects of microgravity, giving a particle speed:

$$v = \sqrt{\frac{2E_e}{\rho z^3}} \quad (12)$$

Figure 5 (left) shows an example set of cracks for a dense 1 m boulder and the resulting number of ejected particles (right). The model predicts layer spacing ranging from ~0.1 to 11 cm and ~0.08 to 13 cm within the top 30 cm of dense and porous boulders, respectively, where exfoliation is expected to occur. This range is consistent with the thickness of exfoliation layers

observed on Earth that are driven or assisted by thermal fatigue [e.g., *Holzhausen*, 1989; *Lamp et al.,* 2017; *Martel*, 2017; *Collins et al.*, 2018] and Bennu [*Molaro et al.,* 2020]. It is also consistent with, though slightly wider in range than, the sizes of particles ejected from Bennu, which range from <1 to ~10 cm [*Lauretta and Hergenrother et al.*, 2019]. The predicted minimum is somewhat lower than observed, suggesting that if thermal fracturing is the driving mechanism for these events some particles may not be resolved in spacecraft images. Layers are thinnest near the surface and generally increase with depth, though not strictly monotonically. Larger boulders have more volume, which leads to a higher total number of cracks. A majority of these are sub-centimeter in size due to the boulders' higher strain energies, but the largest layers reach thicknesses of ≥10 cm. Typically, these boulders had only one layer ≥10 cm thick within the upper 30 cm of their surfaces. Small boulders have fewer total cracks, but more that are centimeters in size. This suggests that, as material is disaggregated from the surface over time, large boulders may tend to show only the one or two thick, underlying layers, whereas smaller boulders might show several layers, each a few centimeters thick. Though, as layers disaggregate, multiple sets of cracks may become superimposed on one another, highlighting the complexity of predicting crack spacing and particle sizes in real boulders.

The predicted number of particles (Figure 5, right) produced by exfoliation of the layers ranges from hundreds of centimeter-scale particles to thousands of sub-centimeter particles. The number of particles grows as the diameter increases and boulders have larger cross sections of material to disaggregate. This is higher than events observed at Bennu, which have produced of order ones to hundreds of particles per event [*Lauretta and Hergenrother et al.*, 2019; *Leonard et al.*, *in press*] (Table A1). However, we will neglect sub-centimeter particles for the time being since not all of these would be resolvable in spacecraft images. This is also a reasonable approximation considering that stresses closest to the surface are lowest in magnitude and therefore

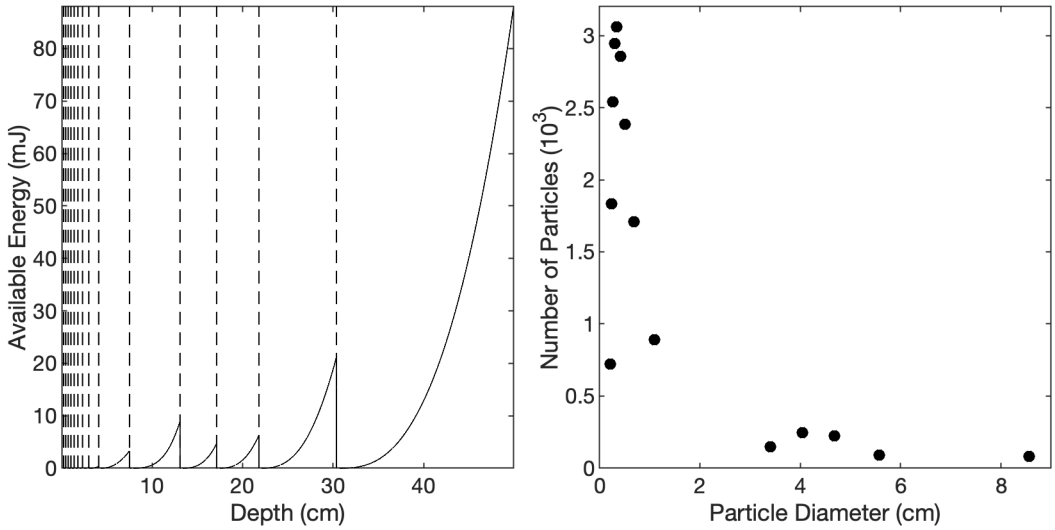

Figure 5. (left) Available energy with depth into the surface of a 1 m boulder per Eq. 9. Dashed lines represent the locations at which cracks form, dropping the available energy to zero. The crack spacing ranges from 0.2 to 8.5 cm. (right) The number of equally sized particles into which flakes disaggregate (Eq. 10), with each having the dimension of the layer thicknesses shown at left.

the smallest exfoliation layers may not meet the required fatigue threshold to develop, and those that do will be removed first from boulder surfaces. Considering only the centimeter-scale (and larger) layers that remain, the number of particles ejected increases from tens in the smallest boulders, to thousands in the largest boulders (Figure 5, right).

The prediction of tens to thousands of ejected particles per event is an upper limit, as an entire exfoliation flake is not realistically expected to disaggregate completely at once. Rather, flakes are expected to break apart over time, and therefore a full boulder cross section is likely to overestimate what may be ejected in a single event. Additionally, the boulder strain energy density is not exactly homogeneous along the radially perpendicular axes and may not possess enough energy to eject particles over its entire cross section, particularly at greater depths and in larger boulders. In some cases, the boulder face where exfoliation occurs may also be less than a full cross section, such as in our ideal boulder whose buried portion of the western hemisphere would be unaffected. Considering these factors, it is more reasonable to expect some fraction of the flake to be ejected, which is also more consistent with observations. For example, an event that disaggregates one quarter of exfoliation flake from a 1-m boulder produces ~225 particles from the 1 cm layer, or ~75 particles from the 3 cm layer below. These are comparable to the largest events observed to date at Bennu. In a larger boulder, the flake fraction must be smaller to produce a similarly sized event. For example, one tenth of a 2 cm exfoliation flake disaggregated from a 5-m boulder produces ~200 particles. Without constraints on crack propagation rates, it is unclear what estimate for the flake fraction is realistic. In this sense, this prediction method gives a reasonable upper bound of tens to hundreds of centimeter-scale particles that can be produced via fatigue for ejection, but the lower bound is not well constrained.

While the calculations above estimate the number of equally sized particles disaggregated from a single layer, it is possible that multiple layers may be sourced during a given ejection event. If the exfoliation layer driving the event is not at the boulder surface, shallower cracks may

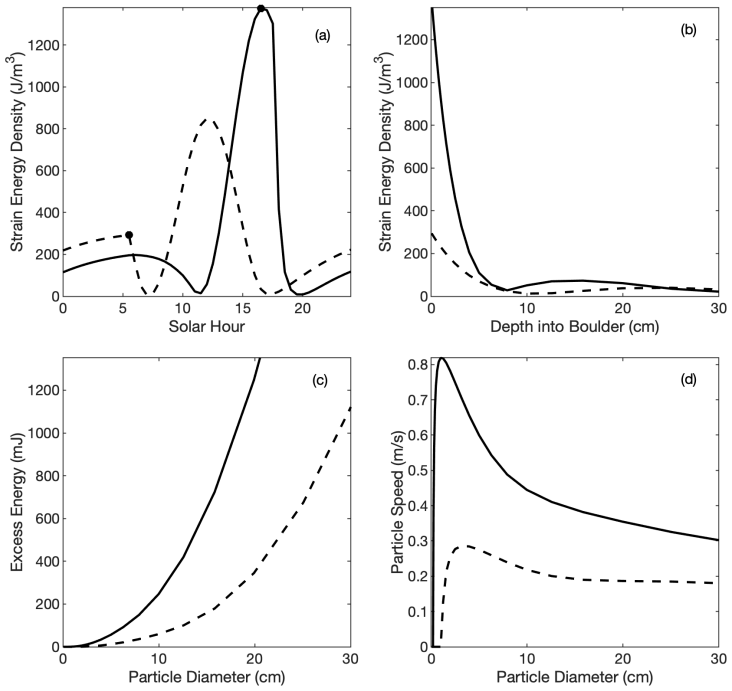

Figure 6. (a) Thermal strain energy density over one solar day at the location of peak thermal strain energy density (solid) and peak tensile stress (dashed) in a 1 m boulder, with the dots showing the time of day at which each occurs. (b) Profiles of the thermal strain energy density with depth from the two locations in (a) to the center of the boulder. (c) Excess energy available in particles with particle size. (d) Ejected particle speed with particle size. The x-axis on panels b and c is limited to the upper 30 cm where exfoliation and surface events are most likely to be initiated.

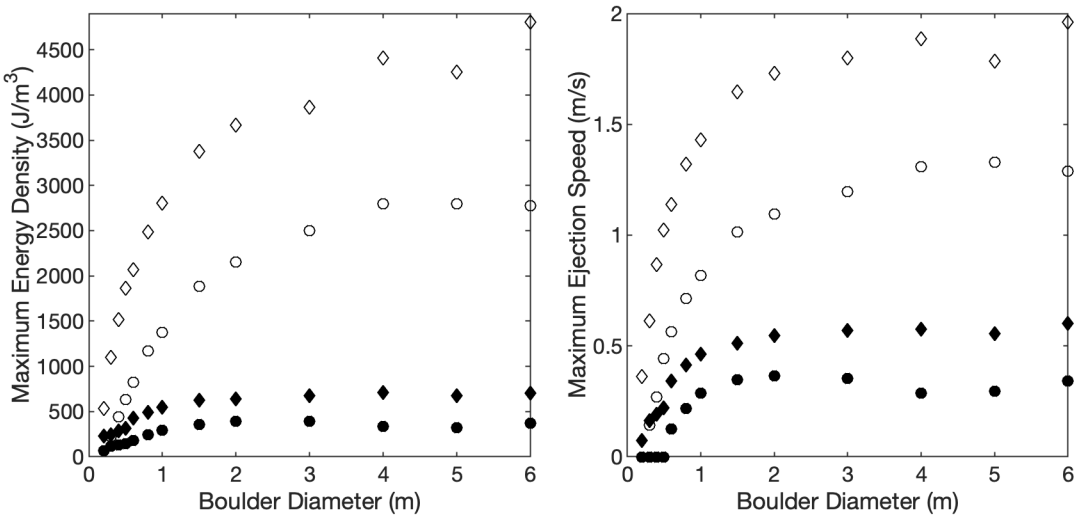

Figure 7. Maximum thermal strain energy density (left) and ejection speed (right) for exfoliation (open) and surface (solid) events in boulders of varying size. Values for dense (circle) and porous (diamonds) boulders show the range of maximum energies and ejection speeds predicted for each type of event.

facilitate breakup of the disaggregated flake into a population of particles with a range of sizes smaller than the flake depth. In this context, or considering the cumulative material disaggregated from boulders across multiple events, the full particle size-frequency distribution (Figure 5, right) gives us a sense of the overall population of particles, and relative number of particle sizes, that we expect to be produced by exfoliation-driven particle ejection events.

Taking the alternate approach, we can calculate particle ejection speeds from the surface of the 1 m boulder independently of the predicted spacing of exfoliation cracks. Figure 6 (a, solid) shows the thermal strain energy density over time at the boulder surface, with peak values in the afternoon an order magnitude higher than at other times of day. At this time (b, solid), the strain energy is highest at the surface and decreases strongly within 10 cm. Taking the depth as our layer thickness, the amount of available energy (c, solid) increases to hundreds of millijoules as particles grow in size. For dense boulders, this leads to particle ejection speeds (d, solid) ranging from ~0.3 to 0.8 m/s, which exceed Bennu's escape speed of ~0.2 m/s, and a minimum ejected particle size of 0.2 mm. We can also estimate particle speeds produced as a result of surface-perpendicular cracks (Figure 6, dashed lines) that develop during the night at boulder surfaces. These may provide a mechanism to break up exfoliation flakes, in which case their surface-perpendicular dimension would still be determined by the exfoliation layer thicknesses. The boulder has less thermal strain energy at this location and time of day, resulting in lower ejection speeds and a minimum ejected particle size of ~2.5 cm. If surface stresses produce cracks that do not interact with exfoliation layers, they may still contribute to the disaggregation of particles, but their spacing (and thus their speeds) cannot be predicted in the same way due to the differing geometry. Overall, this suggests that thermal fatigue can drive ejection events at night on Bennu's surface, but such events may be expected to be lower in energy and with slower-moving particles than those occurring in the afternoon.

Figure 7 shows the maximum energy density (left) and ejection speeds (right) due to exfoliation (open) and surface cracking (solid) for dense boulders (circles) with varying diameter. The maximum ejection speeds are ~1.4 m/s for exfoliation events in large boulders. Ejection

speeds due to surface cracking are much lower and do not occur in boulders <60 cm. Porous boulders have higher strain energy densities and ejection speeds than dense boulders because they have a lower elastic modulus and are less brittle. Since the magnitude of induced stresses are also lower, ejection events are less likely to occur or may occur less frequently in porous materials. The largest porous boulders are most likely to eject particles and have ejection speeds ~30 to 50% higher than the dense boulders, with a maximum of ~2 m/s. The smallest porous boulders have higher speeds by more than a factor of 4 but are the least likely to eject particles due to their low stresses. Overall, these speeds are consistent with particles ejected from Bennu, which ranged from ~0.05 to 3.3 m/s [*Lauretta and Hergenrother et al.*, 2019; *Leonard et al.*, *in press*]. The maximum predicted speed is lower (within a factor of 2) than what is observed, suggesting that although generally fatigue-driven exfoliation is a viable mechanism for particle ejection, there is limited available energy relative to other processes such as impacts [*Bottke et al.*, *in review this collection]*.

The amount of strain energy available in a given boulder varies throughout Bennu's orbit, peaking at perihelion when the diurnal temperature variation is largest. For a 1 m boulder, the change in peak strain energy with solar distance follows an approximate power law relationship with an exponent of –2.1. In contrast to Figure 6, the excess energy available to mobilize particles in a 1 m dense boulder at aphelion decreases to only a few hundred millijoules with a maximum ejection speed of 0.2 m/s. This is similar to the nighttime events, suggesting that the range of energies and ejection speeds for a given boulder size in Figure 7 are also a reasonable approximation for variation throughout the year. Since exfoliation layers are produced progressively, the number and depth of expected layers should realistically reflect some total cumulative energy throughout the entire orbit. On the other hand, stresses are nonlinear with solar distance, and so we might expect crack spacings to skew towards what is expected at perihelion.

The particle sizes determined by Lauretta and Hergenrother et al. [2019] are for spheres, whereas we assume cubes. It would be impractical to assume spherical particles using our methodology because of its reliance on layer spacing to determine the sizes of particles and crack walls. This will have only a minor effect on the comparison of our results to the observations. Most notably, if we approximate that the integration of energy with depth would be the same as performed above and simply split each cube into two smaller spheres, this would increase the number of particles per layer by a factor of 2. However, given the order of magnitude nature of our discussion regarding what fraction of a layer may disaggregate at once, a factor of 2 does not change our conclusion qualitatively. Since halving the volume would also halve the total energy of each particle, this would place a factor of 1/2 in both the numerator and the denominator of Eq. 12. These will cancel out, and therefore the particle speeds shown in Figures 6 and 7 would remain unchanged. Lauretta and Hergenrother et al. [2019] assume a particle density of 2000 kg/m^3 in their calculations, which falls between our solutions for dense and porous boulders.

5 Observational Constraints on Ejection Events

To determine the likelihood of thermal fatigue as a driving mechanism for Bennu's particle ejection events, we must examine our results in the context of both observational constraints and other possible mechanisms. A summary of our results with respect to observational constraints is provided in Table 2, along with the references to which readers can refer for more details regarding the ejection event observational data. A summary the data relevant to this discussion is also included in Appendix B (Table A1). Given the limited dataset and difficulty in accounting for all possible biases, there is uncertainty in some of the possible trends that we discuss. Nevertheless,

the data are compelling to explore and provide an opportunity to perform an initial assessment of the feasibility of our hypothesis.

As described in Section 4, our model of crack spacing and particle ejection due to boulder exfoliation and surface cracking is predicted to produce (i) a range of particle sizes from 1 mm to 13 cm, (ii) a maximum ejection speed of ~2 m/s, and (iii) up to hundreds of ~1 to 10 cm sized particles per event. All three of these results are in good agreement with observations (Table 2), though (iii) is the least well constrained. Our predicted maximum speed falls shy of the maximum observed (3.3 m/s); however, the majority of speeds from the three largest ejection events fall below our best fit profile (Figure 8, left). Since our calculations are based on available energy per particle, the lack of constraints on number of particles does not alter our predicted speeds.

Figure 8 (right, shaded) shows the normalized observed particle size-frequency distribution (SFD) from the three largest eject event observations [*Lauretta and Hergenrother,* 2019] using the upper-limit particle sizes from the observational data (Appendix B), compared to normalized predicted distributions for the 1-m dense boulder (circles) and 6-m porous boulder (diamonds) from our model. A perfect match is not expected, as the total SFD predicted by our model should realistically reflect the cumulative total from all boulders that produce particle ejections, which is not yet known. Nonetheless, the shape of the predicted size-frequency distributions provide a good qualitative match to observations, though quantitatively they skew towards more smaller particles. If Bennu's ejection events are caused by exfoliation, the relative lack of sub-centimeter sized particles could indicate that we are not observing all of the material ejected during any given event, or that the requirements to produce exfoliation layers at sub-centimeter depths is not achieved and therefore such particles should not be produced. A better match is obtained by Chesley et al. [*in review this issue*] who assumed the observed particles are oblate spheroids (Figure 8, unshaded) instead of spheres [*Lauretta and Hergenrother et al.,* 2019]. They used their calculated axis ratio distribution to convert our predicted SFD to oblate particles, shifting the predicted population to larger diameters with a peak at ~0.7 cm. Oblate or rectangular particles are consistent with the exfoliation mechanism, which may disaggregate flakes into fragments with a range of widths. Using rectangular instead of cubic particles in our model would result in a slight increase in predicted ejection speeds, as less energy would be needed to create surface-normal cracks.

Table 2. A summary of our results with respect to constraints from observed particle ejection events at Bennu. Constraints and supporting data are described in detail by Lauretta and Hergenrother et al. [2019], Hergenrother et al. [*in review this collection*], Chesley et al. [*in review this collection*], Leonard et al. [*in press*], and Pelgrift et al. [2020] (Appendix B).

Constraints	**Observations**	**Thermal Fatigue**	**Impacts***
Maximum Particle Speed (m/s)	~3.3	~2	>3.2
Particle Diameters (cm)	<1 to ~10	~0.08 to 13	~7 (upper limit)
Number of Particles	1s to 100s	10s to 100s (upper limit)	unconstrained
Total Mass (g)	1s to 1000s	10s to 1000s (upper limit)	350 (upper limit)
Time of Day	predominantly afternoon & night	afternoon (primary) & night (secondary)	any, afternoon preference
Frequency	days to weeks	unconstrained	biweekly near perihelion
Latitude & Longitude	various	any	any, preference equatorial

*Based on calculations for a 7000-J impact event.

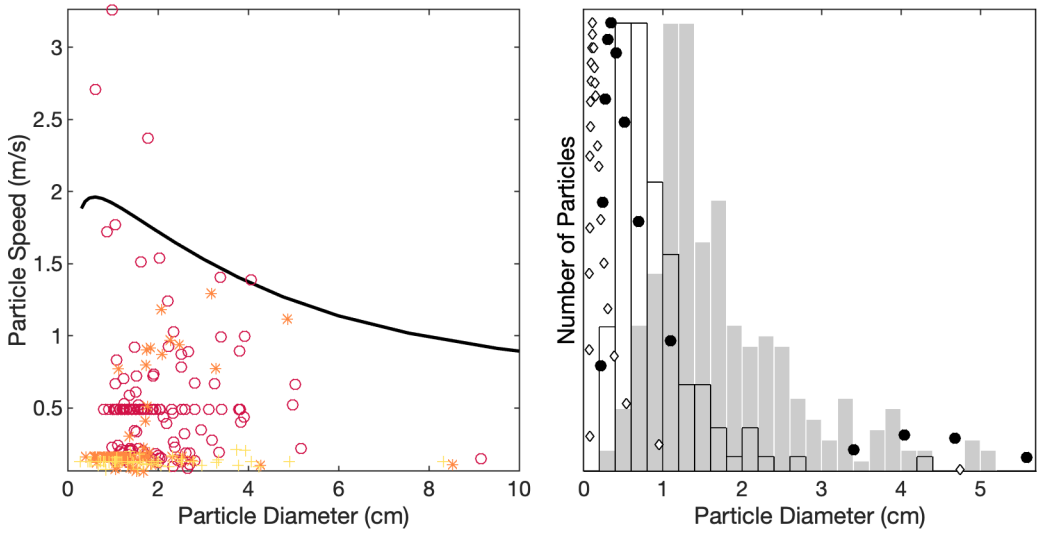

Figure 8. (left) Predicted maximum ejection speed with particle diameter for a 6 m, porous boulder (black line) with particle speeds and upper limit diameters from the three largest ejection events (symbols) as reported by Lauretta and Hergenrother et al. [*2019*] (Appendix B). The groups at ~0.5 and 0.16 m/s are particles with no trajectories for which the mean velocities were assumed. (right) Particle size-frequency distribution for the same ejection events assuming the lowest albedo particles (shaded), and the distribution assuming oblate particles from Chesley et al. [*in review this issue*] (unshaded). The symbols show the predicted distribution produced from a 6 m, porous (circles) and 1 m dense (diamonds) boulder. Each distribution is normalized to its largest bin value.

Additionally, the timing of observed particle ejection events is consistent with the times of day that exfoliation and surface cracking are expected to occur (Figure 9). Strain energy and exfoliation stress for boulders ≥ 1 m are highest during local solar hours 13 to 18, with a peak value at hour 17 (Figure 6; Figure 9). The majority of observed ejection events occur during these times (dashed lines), with four of the five largest events (those with >20 particles) occurring approximately between hours 15 and 18. The event that occurred during local night could have been driven by surface cracking. The hours between sunrise and noon are the least likely for fatigue-driven ejection to occur. As discussed in Section 3.4, these time predictions will vary somewhat between individual boulders when accounting for their unique shapes.

The amount of strain energy available in a given boulder will peak at perihelion and decrease with increasing solar distance. Additionally, annual exfoliation stresses peak ~30 days before perihelion at a solar distance of 0.92 au. It is unlikely that deformation due to annual heating contributes any significant thermal strain energy to boulder surfaces; however, the superposition of annual and diurnal stresses during this time may help overcome fatigue stress thresholds or increase crack propagation rates, leading to more frequent events. Combined, these factors suggest that if Bennu's particle ejection events are driven by thermal fatigue, we should observe more frequent, higher energy events approaching and near perihelion, and less frequent, lower energy events near aphelion. Higher energy events are also expected to produce more, faster moving particles. This is generally supported by the data, which shows that the total energy of events does decrease with increasing solar distance. Though, the five largest events are spread out over several months with lower energy events in between. Events with speeds exceeding 1 m/s have also been

observed at solar distances ≳1.3 au [*Pelgrift et al.,* 2020]. This is not consistent with our predicted decrease in particle speeds near aphelion. More observations are needed to better explore this idea.

While the observations of particle ejection events at Bennu are consistent with what we predict from thermal fatigue, other candidate mechanisms have not been ruled out. In particular, electrostatic lofting and impacts have been considered as alternatives for Bennu, though other mechanisms are also explored generally by Jewitt et al. [2015]. Hartzell et al. [*in review this collection*] report that, depending on the surface cohesion, electrostatic lofting is capable of stripping Bennu of submillimeter sized particles during the day, but cannot produce the large, fast particles observed leaving Bennu's surface during the largest ejection events. Ultimately, they conclude that it is unlikely to cause Bennu's daytime ejection events but cannot be ruled out as a mechanism for smaller events that occur during the night. This leaves impacts as the most reasonable alternative candidate to thermal fatigue (Table 2).

Bottke et al. [*in review this collection]* predicted that 7000-J meteoroid impacts at Bennu should occur on a biweekly cadence near perihelion with a preference to strike in the late afternoon, which is a reasonable match to the timing of the three largest ejection events observed. They found that these impacts, on average, can produce up to 350 g of ejecta, with 80% of the mass having a speed <3.2 m/s if they assume that the impacts strike into cohesionless (1 kPa) soil. This ejecta mass is consistent with low to midrange values of the total masses of observed ejection events, though it can only produce the largest observed individual particles if ejected as a single combined mass (maximum of ~4-7 cm diameter). In this context, the impact hypothesis may be somewhat mass-limited compared to the largest ejection events, but the available energy is more than enough to produce observed ejection speeds. This is in contrast to thermal fatigue, which can potentially produce an excess number of particles relative to observations, but with maximum speeds less than the fastest observed particles. This being said, Bottke et al. [*in review this collection]* only perform calculations for 7000-J impact events (Table 2), which does not capture the probabilistic variation in impactor energy and size that occurs in reality. The limited number of ejection event observations are insufficient to perform any statistical analysis that may provide a better comparison to their results. Both hypotheses predict that impact frequency should decrease towards aphelion.

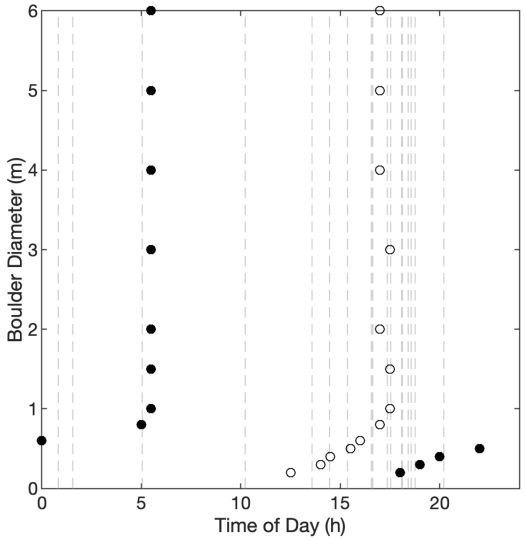

Figure 9. Time of day at which peak surface (solid) and exfoliating or near-surface (open) stress occurs in boulders of varying diameter. The dashed lines show the times of nine ejection events observed at Bennu (see Appendix B).

One weakness in the impact hypothesis is the nature of the impactor target. The cohesive strength of rock is equal to its shear strength under zero confining pressure and typically is the same order of magnitude as its tensile strength. The impact model uses dry sand as an analog for cohesionless material, which has a cohesive strength two orders of magnitude lower than even weak and porous intact rock [e.g., *Burk*, 1964; *Grott et al.*, 2019]. Bottke et al. [*in review this collection]* report that impacts occurring into cohesionless material can produce the observed mass or particle speeds from the three largest ejection events, but impacts into intact rock cannot. However, the majority of Bennu's surface is covered with intact boulders that have enough strength to sustain visible fractures and therefore cannot be considered cohesionless. Further, they report that an impact into cohesionless soil should produce a crater at least 14 cm wide, which would excavate at least 260 cm^3 of material and require a soil depth of 3 to 4 cm to occur (assuming its shape is a spherical shell). Both of these factors suggest that only a fraction of Bennu's surface has properties suitable to produce impact events consistent with ejection event observations, which would lead to a less frequent cadence of ejection events than they report and therefore provide a worse match to observations. On the other hand, the nature of impacts into rubble pile surfaces is not well understood, and it is unclear at what size materials transition from unconsolidated small pebbles to intact boulders that are adjacent to each other, or how these regimes are influenced by impactor energy.

While fatigue provides a good match to observational constraints at the present time, more observations are needed to explore long term variation in the mass, energy, and frequency of particle ejection events. Additional work studying exfoliation features on Bennu's surface will also provide better constraints on fatigue thresholds and lead to more accurate predictions of mass disaggregation rates from our model. It is also likely that fatigue works in synergy with both impacts and electrostatic lofting to produce the asteroid surface we see, and all three mechanisms may contribute to observed ejection events. For example, if stress magnitudes are sufficient for exfoliation they can produce sub-centimeter sized layers, electrostatic lofting could help sweep away the smallest disaggregated particles to leave behind the underlying centimeter scale layers we see in boulder surfaces. Such an interaction could help to explain the lack of sub-centimeter sized particles in observed ejection events relative to the particle population predicted by our model. Because exfoliation flakes develop progressively, fatigue may also provide planes of weakness that meteoroid impacts can exploit. Even if the ejection events are ultimately driven by impact processes, it is likely that the exfoliation layers play a strong role in the particle size distribution of impact ejecta both leaving and remaining on Bennu's surface. The popping up of an exfoliation layer's edge over a curved surface could also loft loose particles resting on the boulder [*Jawin et al.* submitted] from impact and/or other thermal mechanisms, even if the exfoliation flake itself does not disaggregate.

6 Conclusions

We performed finite element simulations of stress fields in serpentine-rich carbonaceous chondrite boulders undergoing diurnal thermal cycling on the surface of Bennu. We find their magnitudes to be comparable to the tensile strength of terrestrial analog materials. These stresses are sufficient to drive thermal fatigue (a subcritical crack growth process) and possibly other thermal fracturing processes (e.g., thermal shock) on the surface. The occurrence of thermal fatigue has been substantiated by the widespread observation of fatigue-driven exfoliation on Bennu [*Molaro et al.,* 2020], which likely works in combination with shallow surface-normal cracking to

drive boulder breakdown. Large-scale through-going fractures from fatigue likely also develop, but more work is needed to map fracture orientations across the surface to assess latitudinal trends. Annual stresses arising throughout Bennu's orbit may interact with diurnal effects, influencing the rate and/or location of crack propagation in large boulders, though better constraints on the stress threshold required to drive fatigue in carbonaceous chondrite materials are needed to explore such effects. Thermal fatigue likely plays a dominant role in Bennu's landscape evolution, and future work to identify and study fatigue-driven features will provide valuable insights into the rate at which the process occurs and how it interacts with other surface processes. Analysis of returned samples will also provide better constraints on the thermal and mechanical properties of Bennu's surface materials, which have a critical bearing on induced thermal stress.

We posit that the process of exfoliation can lead to the energetic ejection of particles from the asteroid surface as a fatigue crack moves from sub-critical to critical failure at the end of its life. We quantified the thermal strain energy stored by boulders during the times of day at which exfoliation is expected to occur to predict the characteristic spacing of exfoliation layers. We find that layers should be thinnest near the boulder surface where the strain energy is highest and increase with depth, with predicted crack spacings of order 1 mm to 10 cm. This is consistent with observations of exfoliation layers on Bennu's boulders [*Molaro et al.*, 2020], as well as in terrestrial environments [e.g., *Holzhausen*, 1989; *Fletcher et al.*, 2006; *Martel*, 2017]. We find that exfoliation flakes can disaggregate into an upper limit of hundreds of centimeter-scale particles, although this result is less well constrained. The ejection speed of these mobilized particles is predicted to increase with decreasing diameter and to have a maximum value of ~2 m/s for porous boulders. Dense boulders have a lower maximum speed of ~1.3 m/s. For both porous and dense materials, ejection speeds generated during surface cracking events at night are much lower than predicted during exfoliation events.

These predictions are in good agreement with the sizes and speeds of particles from ejection events observed at Bennu to date by the OSIRIS-REx spacecraft [*Lauretta and Hergenrother et al.*, 2019; *Leonard et al.*, in press]. The shape of the size-frequency distribution of the particle population that exfoliation is predicted to produce is also consistent, though it skews toward a greater number of sub-centimeter particles than is observed. If fatigue-driven exfoliation is driving the observed ejection events, this would indicate that we are not observing all of the particles ejected, which is possible given the limitations of our detection capability [*Hergenrother et al.,* in review this issue]. It could also indicate that the fatigue threshold is not met near the boulder surface and therefore sub-centimeter exfoliation layers are not produced. More observations are needed to confirm whether the predicted trends of increasing event frequency and/or energy during perihelion approach occurs.

If thermal fatigue indeed plays a role in Bennu's activity, this has broad implications for our understanding of active asteroids and the asteroid population as a whole. Previous works have hypothesized that thermal fracture processes may generate activity on active asteroids with small perihelion distances, such as (3200) Phaethon [*Jewitt and Li*, 2010]. Our results support this hypothesis. With a diurnal temperature variation of hundreds of degrees, Phaethon's surface is likely to be subject to thermal shock processes, with fatigue operating at depth to weaken and prepare the rock for disruption. However, the fact that thermal fatigue alone may be capable of generating activity suggests that there may be many more active asteroids than are currently known, likely including many in near-Earth space. With less energetic activity, a lack of tails or comae would make such bodies hard to identify from ground-based observations, and previous missions to visit asteroids up close lacked the capability to detect ejection events like those

observed on Bennu. Objects with a similar rotation period and composition to Bennu should begin generating strain energies capable of ejecting particles at solar distances of ~1.5 to 2 au. This activity "line" for different bodies will vary primarily with composition, as an object's mechanical properties control how it responds to thermal forcing. Fatigue may also become possible on some bodies at greater distances than activity can occur, for example because the strain energy is insufficient to mobilize particles in a given gravity environment. There is much to be learned about how this process operates. For example, it is unclear what roles crack propagation distance and rate play in producing ejection events, or to what extent breakup of exfoliation flakes occurs during such an event or beforehand. A better understanding of these ideas will provide valuable insights into the distribution of active asteroids in the solar system and their mass loss rates, which has implications for asteroid survival times and the production of interplanetary debris.

Appendix A: Influence of Boulder Shape

Although real boulders are not necessarily well approximated by spheres, our choice to use spherical boulders does not qualitatively change our results. Boulder shape can influence the nature of thermal fatigue in two primary contexts: face orientation and surface/shape roughness. In both cases, realistic shapes will cause variations in the magnitude and timing of thermally induced stresses experienced by different parts of the boulder. To explore these effects, we simulated a 1 m square boulder embedded at an angle in the regolith and a 1 m spherical boulder with 10 cm deep triangular surface "cracks" spaced 10 cm apart (Figure A1). The variation in stress magnitudes in each case (described below) is smaller than ±25%, which is comparable to their uncertainty values and to stress sensitivity to variation in mechanical properties [*Molaro et al.*, 2017]. No color scale is included in Figure 1A because these simulations were performed at a lower resolution for computational efficiency, and so this stress variation represents an upper limit on behavior.

Surface stresses are primarily influenced by surface orientation. For boulders that are especially angular, the orientation of an individual face with respect to the Sun's location and direction of motion will influence the timing and amount of incident solar radiation it receives. For example, the square boulder (Figure A1, top) has a highly sloped east face, which will heat very quickly at sunrise, but it will also become self-shadowed earlier in the day than a lower-sloped surface. This will cause it to experience a lower diurnal temperature variation and a reduction in the magnitude of surface stress. This effect may be enhanced by the fact that it has more surface area from which to emit radiation compared to a sphere. An increase in local surface curvature at a given location due to surface roughness or bumps can also lead to decreased surface stress.

Exfoliation stresses are influenced primarily by boulder shape, depending on the scale of surface or shape roughness. Exfoliation fractures will develop underneath small-scale surface bumps and may leave behind a smoother surface after the flake disaggregates. As the roughness of the shape approaches the scale of a few thermal skin depths, different portions of the boulder may begin to behave like separate segments, with exfoliation occurring independently on each. For example, the square boulder (Figure A1, b) has two local maximums in exfoliation stress at each corner that peak at two different times of day. The stress orientation near each corner is still surface-normal in this case, and the surface-parallel crack propagation could serve to round them over time. The stress orientation between corners is more difficult to describe with respect to the boulder's angular shape. Below the exfoliation depth the stress orientation is determined by which boulder faces provide the most efficient pathway for cooling. In spherical boulders, this is N-S, but in this case the stress between the two corners is roughly E-W. This aligns with the surface-normal stress at the western corner and may lead the boulder to develop a flat western face. The stress magnitude is also enhanced at the western corner (relative to a spherical boulder) due to the corner orientation with respect to the time at which the boulder is hottest. In this sense, exfoliation is also influenced by surface orientation to the extent that it determines which boulder faces experience exfoliation and how they heat. In contrast, the exfoliation stress field in Figure A1 (d) remains largely unchanged from a spherical boulder, and the stress orientation in the "bumps" remains normal to the spherical shape of the surface as if the cracks did not exist. In this case exfoliation would serve to cut through or under the bumps. There is nuance in how the stress fields change and behave in irregular objects and much to still be learned about the evolution of boulder shapes from thermal fracturing.

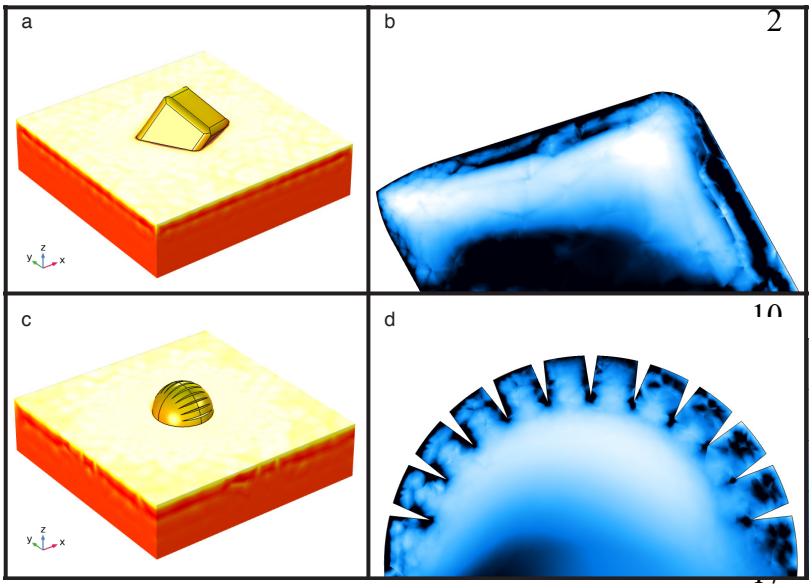

Figure A1. (a) Temperature of a square 1 m boulder in the midafternoon being heated by the Sun as it moves within the y plane, and (b) a cross section through the boulder along the y plane. Panels (c) and (d) show the same for a spherical boulder with 10 cm surface "cracks."

Appendix B: Summary of observational data

Table A1 summarizes some of the relevant data from seventeen particle ejection events observed between January 6 and September 14 of 2019. These data are compiled from Lauretta and Hergenrother et al. [2019], Hergenrother et al. [*in review this collection*], Chesley et al. [*in review this issue*], Leonard et al. [in press], and Pelgrift et al. [2020] for use in Figures 8 and 9, Table 2, and the text in Section 5. Table 1A reports the number of *observed* particles during each ejection event, which may differ from the number of *analyzed* particles in the aforementioned studies. The photometry techniques used to estimate particle sizes were performed using a range of assumed particle albedos. Following the methodology described by Lauretta and Hergenrother et al. [2019], we use a density of 2000 kg/m^3 and an albedo of 0.033 to provide an upper-limit estimate on observed particle diameters for Figure 8. Tables 2 and A1 show values assuming an albedo of 0.044, which yields a midrange estimate of particle sizes. Note that Lauretta and Hergenrother et al. [2019] and Hergenrother et al. [*in review this collection*] make different assumptions about particle shape, and therefore these data (Table 1A) are only intended as a an approximate guide to characteristic particle sizes observed. More complete datasets are available in the aforementioned references. We also caution that the total number of observed events is limited, making it difficult to assess how statistically meaningful any specific trends may be. There may also be biases in the timing of observed events, and the number and albedo of observed particles, resulting from spacecraft location, orientation, distance from the asteroid, and other factors.

Table A1. Subset of data from the particle ejection events observed at Bennu compiled from Lauretta and Hergenrother et al. [2019][1], Hergenrother et al. [*in review this issue*][2], Chesley et al. [*in review this issue*][3], Leonard et al. [in press][4], and Pelgrift et al. [2020][5].

Event Date	Solar Distance (au)	Solar Hour	No. Observed Particles	Maximum Speed (m/s)	Total Energy (mJ)	Total Mass (g)	Particle Diameter (cm)			References
							Ave	Min	Max	
6 Jan	0.89	15.36	200	3.3	270	1800	1.2	0.2	5-8	1, 2
19 Jan	0.89	16.63	108	1.3	100	600	1	0.5	4-7	1, 2, 3
29 Jan	0.90	18.76	≲10	<0.5						2, 4
4 Feb	0.92	18.41	≲10	<0.5						2, 4
5 Feb	0.92	17.36	≲10	<0.5						2, 4
8 Feb	0.93	14.46	≲10	<0.5						2, 4
8 Feb	0.93	1.56	≲10	<0.5						2, 4
11 Feb	0.93	18.08	72	0.2	8	700	1.2	0.3	4-7	1, 2, 3
15 Feb	0.94	0.83	≲10	<0.5				0.3	1	2
19 Apr	1.14	16.56	22	0.9				0.7	5	2, 4, 5
18 Jun	1.29	17.53	≲10	1.6				0.3	0.6	2, 5
16 Aug	1.35	20.2	≲10	<0.5				1.2	1.4	2, 3
23 Aug	1.35	18.12	≲10	<0.5				0.9	2.6	2, 3, 5
28 Aug	1.35	18.56	≲10	<0.5				0.2	0.3	2, 3
05 Sep	1.35	13.58	≲10	<0.5				0.6	1.2	2, 3
13 Sep	1.34	10.22	30	2.3				0.5	1.9	2, 3, 5
14 Sep	1.34	5.05	≲10	<0.5				0.6	0.9	2, 3

References

Altindag, R., A. G. S. R. A. Essays (2010), Predicting the relationships between brittleness and mechanical properties (UCS, TS and SH) of rocks, *Scientific research and Essays 5.16*, 2107-2118.

Barnouin, O. S. et al. (2019), Shape of (101955) Bennu indicative of a rubble pile with internal stiffness, *Nat. Geosci.*, *12*(4), 247–252, doi:10.1038/s41561-019-0330-x.

Basilevsky, A. T., J. W. Head, F. Horz, and K. Ramsley (2015), Survival times of meter-sized rock boulders on the surface of airless bodies, *Planetary Space Sci.*, *117*(C), 312–328, doi:10.1016/j.pss.2015.07.003.

Bottke, W. F. et al. (n.d.), Meteoroid Impacts as a Source of Bennu's Particle Ejection Events, *J. Geophys. Res. Planets*, *in review this collection*.

Browning, J., Meredith, P., & Gudmundsson, A. (2016). Cooling-dominated cracking in thermally stressed volcanic rocks. *Geophysical Research Letters*, *43*(16), 8417–8425. http://doi.org/10.1002/2016GL070532

Burk, C. (1964), A study of serpentinite: the AMSOC core hole near Mayaguez, Puerto Rico, *National Academy of Sciences-Nat. Res. Council Publ*, *1*, 188.

Chen, C.-S., E. Pan, and B. Amadei (1998), Determination of deformability and tensile strength of anisotropic rock using Brazilian tests, *Int. J. Rock Mech. Mining Sci.*, *35*(1), 43–61, doi:10.1016/S0148-9062(97)00329-X.

Chesley, S. R. et al., Trajectory estimation for particles observed in the vicinity of (101955) Bennu. *Journal of Geophysical Research: Planets*, (*in review this collection*).

Christensen, N. I. (1966), Elasticity of ultrabasic rocks, *J. Geophys. Res. Planets*, *71*(24), 5921–5931, doi:10.1029/JZ071i024p05921.

Collins, B. D., and G. M. Stock (2016), Rockfall triggering by cyclic thermal stressing of exfoliation fractures, *Nat. Geosci.*, *9*(5), 395–400, doi:10.1038/ngeo2686.

Collins, B. D., G. M. Stock, M. C. Eppes, S. W. Lewis, S. C. Corbett, and J. B. Smith (2018), Thermal influences on spontaneous rock dome exfoliation, *Nat. Commun.*, *9*(1), 1–12, doi:10.1038/s41467-017-02728-1.

Collins, B. D., Stock, G. M., and Eppes, M. C. (2019). Relaxation Response of Critically Stressed Macroscale Surficial Rock Sheets. *Rock Mechanics and Rock Engineering*, 1–11. http://doi.org/10.1007/s00603-019-01832-6

Colwell, J. E., S. Batiste, M. Horányi, S. Robertson, and S. Sture (2007), Lunar surface: Dust dynamics and regolith mechanics, *Reviews of Geophysics*, *45*(2), RG2006, doi:10.1029/2005RG000184.

Delbo, M., G. Libourel, J. Wilkerson, N. Murdoch, P. Michel, K. T. Ramesh, C. Ganino, C. Verati, and S. Marchi (2014), Thermal fatigue as the origin of regolith on small asteroids, *Nature*, *508*(7495), 233–236, doi:10.1038/nature13153.

DellaGiustina, D. N., J. P. Emery et al. (2019), Properties of rubble-pile asteroid (101955) Bennu from OSIRIS-REx imaging and thermal analysis, *Nat. Astron.*, *3*(4), 341–351, doi:10.1038/s41550-019-0731-1.

Dombard, A. J., O. S. Barnouin, L. M. Prockter, and P. C. Thomas (2010), Boulders and ponds on the Asteroid 433 Eros, *Icarus*, *210*(2), 713–721, doi:10.1016/j.icarus.2010.07.006.

Drief, A., and F. Nieto (1999), The Effect of Dry Grinding on Antigorite from Mulhacen, Spain, *Clays Clay Miner.*, *47*(4), 417–424, doi:10.1346/CCMN.1999.0470404.

Emmerich, F. G. (2007). Tensile strength and fracture toughness of brittle materials. *Journal of Applied Physics*, *102*(7), 073504–13. http://doi.org/10.1063/1.2785008

Eppes, M. C., A. Willis, J. Molaro, S. Abernathy, and B. Zhou (2015), Cracks in Martian boulders exhibit preferred orientations that point to solar-induced thermal stress, *Nat. Commun.*, *6*, 6712, doi:10.1038/ncomms7712.

Eppes, M. C., and R. Keanini (2017), Mechanical weathering and rock erosion by climate-dependent subcritical cracking, *Reviews of Geophysics*, *55*(2), 470–508, doi:10.1002/2017RG000557.

Eppes, M. C., B. Magi, B. Hallet, E. Delmelle, P. Mackenzie-Helnwein, K. Warren, and S. Swami (2016), Deciphering the role of solar-induced thermal stresses in rock weathering, *Geol. Soc. Am. Bull.*, B31422.1–24, doi:10.1130/B31422.1.

Eppes, M. C., L. D. McFadden, K. W. Wegmann, and L. A. Scuderi (2010), Cracks in desert pavement rocks: Further insights into mechanical weathering by directional insolation, *Geomorphology*, *123*(1-2), 97–108, doi:10.1016/j.geomorph.2010.07.003.

Fletcher, R., H. Buss, and S. Brantley (2006), A spheroidal weathering model coupling porewater chemistry to soil thicknesses during steady-state denudation, *Earth and Planetary Science Letters*, *244*(1-2), 444–457, doi:10.1016/j.epsl.2006.01.055.

Graves, K.J., Minton, D.A., Molaro, J.L. and Hirabayashi, M., 2019. Resurfacing asteroids from thermally induced surface degradation. *Icarus*, *322*, pp.1-12.

Grott, M. et al. (2019), Low thermal conductivity boulder with high porosity identified on C-type asteroid (162173) Ryugu, *Nat. Astron.*, *5*, 1–6, doi:10.1038/s41550-019-0832-x.

Hamilton, V. E. et al. (2019), Evidence for widespread hydrated minerals on asteroid (101955) Bennu, *Nat. Astron.*, *3*(4), 332–340, doi:10.1038/s41550-019-0722-2.

Hartzell, C. M. et al., An Evaluation of Electrostatic Lofting as an Active Mechanism on Bennu, *J. Geophys. Res. Planets*, *in review this collection*.

Hazeli, K., C. El Mir, S. Papanikolaou, M. Delbo, and K. T. Ramesh (2018), The origins of Asteroidal rock disaggregation: Interplay of thermal fatigue and microstructure, *Icarus*, *304*, 172–182, doi:10.1016/j.icarus.2017.12.035.

Hergenrother, C.W., et al., *J. Geophys. Res. Planets*, *in review this collection*.

Hergenrother, C.W., Maleszewski, C.K., Nolan, M.C., Li, J.Y., d'Aubigny, C.D., Shelly, F.C., Howell, E.S., Kareta, T.R., Izawa, M.R.M., Barucci, M.A. and Bierhaus, E.B., 2019. The operational environment and rotational acceleration of asteroid (101955) Bennu from OSIRIS-REx observations. *Nature Communications*, *10*(1), p.1291.

Holzhausen, G. R. (1989), Origin of sheet structure, 1. Morphology and boundary conditions, *Eng. Geol.*, *27*(1-4), 225–278, doi:10.1016/0013-7952(89)90035-5.

Horai, K.-I. (2012), Thermal conductivity of rock-forming minerals, *J. Geophys. Res.*, *76*(5), 1278–1308, doi:10.1029/JB076i005p01278.

Howard, K. T., et al. (2009). Modal mineralogy of CM2 chondrites by X-ray diffraction (PSD-XRD). Part 1: Total phyllosilicate abundance and the degree of aqueous alteration. *Geochimica et Cosmochimica Acta 73.15:* 4576-4589.

Jansen, D. P., Carlson, S. R., & Young, R. P. (1993). Ultrasonic imaging and acoustic emission monitoring of thermally induced microcracks in Lac du Bonnet granite. *Journal of Geophysical Research*, *98*(B12), 22231–22243.

Janssen, M., Zuidema, J. and Wanhill, R.J.H., 2002. Fracture Mechanics, 2-nd Edition. *Delft DUP Blue Print*.

Jewitt, D., and J. Li (2010), Activity in Geminid Parent (3200) Phaethon, *Astron. J.*, *140*(5), 1519.

Jewitt, D., H. Hsieh, and J. Agarwal (2015), The active asteroids, in *Asteroids IV*, University of Arizona Press, 221-241.

Kendrick, K. J., Partin, C. A., & Graham, R. C. (2016). Granitic Boulder Erosion Caused by Chaparral Wildfire: Implications for Cosmogenic Radionuclide Dating of Bedrock Surfaces. *The Journal of Geology*, *124*(4), 529–539. http://doi.org/10.1086/686273

Kranz, R. L. (1979), Crack-crack and crack-pore interactions in stressed granite, *Int. J. Rock Mech. Mining Sci. Geomech. Abs.*, *16*(1), 37–47, doi:10.1016/0148-9062(79)90773-3.

Krokosky, E. M., and A. Husak (1968), Strength characteristics of basalt rock in ultra-high vacuum, *J. Geophys. Res.*, *73*(6), 2237–2247, doi:10.1029/JB073i006p02237.

Lamp, J. L., Marchant, D. R., Mackay, S. L., & Head, J. W. (2017). Thermal stress weathering and the spalling of Antarctic rocks. *Journal of Geophysical Research: Earth Surface*, *122*(1), 3–24. http://doi.org/10.1002/2016JF003992

Lantz, C., R. Brunetto, M. A. Barucci, and E. D. Astronomy (2015), Ion irradiation of the Murchison meteorite: Visible to mid-infrared spectroscopic results. *Astronomy & Astrophysics, 577*, A41.

Lauretta, D. S., C. W. Hergenrother, et al. (2019), Episodes of Particle Ejection From the Surface of the Active Asteroid (101955) Bennu, *Science*, *366*(6470), 10.1126/science.aay3544.

Lauretta, D.S., DellaGiustina, D.N., Bennett, C.A., Golish, D.R., Becker, K.J., Balram-Knutson, S.S., Barnouin, O.S., Becker, T.L., Bottke, W.F., Boynton, W.V. and Campins, H. (2019). The unexpected surface of asteroid (101955) Bennu. *Nature*, *568*(7750), 55-60.

Lawn, B. (1993), *Fracture of brittle solids*, Cambridge, UK: Cambridge University Press.

Ledlow, M. J., M. Zeilik, J. O. Burns, and G. R. Gisler (1992), Subsurface emissions from Mercury-VLA radio observations at 2 and 6 centimeters, *Astron. J.*, *384*, 640–655.

Leonard, J. M., et al., (in press) Initial Orbit Determination and Event Reconstruction from Estimation of Particle Trajectories about (101955) Bennu, *in press with Earth and Space Science.*

Levi, F. A. (1973), Thermal Fatigue: A possible source of structural modifications in meteorites, *Meteoritics*, *8*(3), 209–221, doi:10.1111/j.1945-5100.1973.tb01250.x.

Li, Y., A. T. Basilevsky, M. Xie, and W.-H. Ip (2017), Shape of boulders ejected from small lunar impact craters, *Planetary Space Sci.*, *145*, 71–77, doi:10.1016/j.pss.2017.07.014.

Macke, R. J., G. J. Consolmagno, and D. T. Britt (2011), Density, porosity, and magnetic susceptibility of carbonaceous chondrites, *Meteoritics*, *46*(12), 1842–1862, doi:10.1111/j.1945-5100.2011.01298.x.

Martel, S. J. (2011), Mechanics of curved surfaces, with application to surface-parallel cracks, *Geophys. Res. Lett.*, *38*(20), L20303, doi:10.1029/2011GL049354.

Martel, S. J. (2017), Progress in understanding sheeting joints over the past two centuries, *Journal of Structural Geology*, *94*, 68–86, doi:10.1016/j.jsg.2016.11.003.

McFadden, L. D., M. C. Eppes, A. R. Gillespie, and B. Hallet (2005), Physical weathering in arid landscapes due to diurnal variation in the direction of solar heating, *Geol. Soc. America. Bull.*, *117*(1), 161, doi:10.1130/B25508.1.

McKinstry, H. A. (1965), Thermal expansion of clay minerals, *American Mineralogist*, *50*(1-2), 212–222.

El Mir, C., K. T. Ramesh, and M. Delbo (2019), The efficiency of thermal fatigue in regolith generation on small airless bodies, *Icarus*, *333*, 356–370, doi:10.1016/j.icarus.2019.06.001.

Molaro, J. L. et al. (n.d.), In situ evidence of thermally induced rock breakdown widespread on Bennu's surface, *Nature Communications*, *11*(1), 1-11, doi:10.1038/s41467-020-16528-7

Molaro, J. L., S. Byrne, and J. L. Le (2017), Thermally induced stresses in boulders on airless body surfaces, and implications for rock breakdown, *Icarus*, *294*, 247–261, doi:10.1016/j.icarus.2017.03.008.

Molaro, J. L., S. Byrne, and S. A. Langer (2015), Grain-scale thermoelastic stresses and spatiotemporal temperature gradients on airless bodies, implications for rock breakdown, *J. Geophys. Res. Planets*, *120*(2), 255–277, doi:10.1002/2014JE004729.

Molaro, J., and S. Byrne (2012), Rates of temperature change of airless landscapes and implications for thermal stress weathering, *J. Geophys. Res. Planets*, *117*(E10), doi:10.1029/2012JE004138.

Nakamura, T. (2005), Post-hydration thermal metamorphism of carbonaceous chondrites, *Journal of Mineralogical and Petrological Sciences*, *100*(6), 260–272, doi:10.2465/jmps.100.260.

Opeil, C. P., G. J. Consolmagno, and D. T. Britt (2010), The thermal conductivity of meteorites: New measurements and analysis, *Icarus*, *208*(1), 449–454, doi:10.1016/j.icarus.2010.01.021.

Pelgrift, J. Y. et al. (2020), Reconstruction of Bennu Particle Events from Sparse Data, *Earth and Space Science*, p.e2019EA000938, doi:10.1029/2019EA000938.

Richter, D., and G. Simmons (1974), Thermal expansion behavior of igneous rocks, *Mechanics and Mining Sciences & Geomechanics*, *11*(10), 403–411, doi:10.1016/0148-9062(74)91111-5.

Rozitis, B. et al. (2020), Global temperatures of asteroid (101955) Bennu and implications for particle ejection, *J. Geophys. Res. Planets*, e2019JE006323, doi: 10.1029/2019JE006323.

Ruesch, O., Sefton-Nash, E., Vago, J. L., Küppers, M., Pasckert, J. H., Khron, K., & Otto, K. (2020). In situ fragmentation of lunar blocks and implications for impacts and solar-induced thermal stresses. *Icarus*, *336*, 113431. http://doi.org/10.1016/j.icarus.2019.113431

Sanio, H. P. (1985), Prediction of the performance of disc cutters in anisotropic rock, *Int. J. of Rock Mech. and Mining Sci. & Geomech. Abstracts*, *22*(3), 153–161, doi:10.1016/0148-9062(85)93229-2.

Tenthorey, E. and Cox, S.F., (2003), Reaction-enhanced permeability during serpentinite dehydration. *Geology*, *31*(10), pp.921-924.

Thirumalai, K., and S. G. Demou (1970), Effect of Reduced Pressure on Thermal-Expansion Behavior of Rocks and Its Significance to Thermal Fragmentation, *J. Appl. Phys.*, *41*(13), 5147–5151, doi:10.1063/1.1658636.

Thompson, M. S., M. J. Loeffler, R. V. Morris, Keller, L. P., and R. Christoffersen (2019), Spectral and chemical effects of simulated space weathering of the Murchison CM2 carbonaceous chondrite, *Icarus*, *319*, 499–511, doi:10.1016/j.icarus.2018.09.022.

Vasavada, A. R., J. L. Bandfield, B. T. Greenhagen, P. O. Hayne, M. A. Siegler, J. P. Williams, and D. A. Paige (2012), Lunar equatorial surface temperatures and regolith properties from the Diviner Lunar Radiometer Experiment, *J. Geophys. Res.*, *117*(E12), E00H18, doi:10.1029/2011JE003987.

Walsh, K. J. et al. (2019), Craters, boulders and regolith of (101955) Bennu indicative of an old and dynamic surface, *Nat. Geosci.*, *12*(4), 242–246, doi:10.1038/s41561-019-0326-6.

Walsh, S. D. C., and I. N. Lomov (2013), Micromechanical modeling of thermal spallation in granitic rock, *Int. J. Heat Mass Transf.*, *65*(C), 366–373, doi:10.1016/j.ijheatmasstransfer.2013.05.043.

Wang, P., Xu, J., Liu, S., & Wang, H. (2016). Dynamic mechanical properties and deterioration of red-sandstone subjected to repeated thermal shocks. *Engineering Geology*, *212*, 1–9. http://doi.org/10.1016/j.enggeo.2016.07.015

Waragai, T. (1998), Effects of rock surface temperature on exfoliation, rock varnish, and lichens on a boulder in the Hunza Valley, Karakoram Mountains, Pakistan, *Arctic and alpine research, 30*(2), 184-92.

Acknowledgments, Samples, and Data

We are grateful for the tremendous amount of work done by the entire OSIRIS-REx Team that made the encounter with Bennu possible and facilitated the collection of the scientific data that was used in this work. We also thank the editor for the OSIRIS-REx Team, Catherine Wolner, for helping us prepare this manuscript for publication. This material is based upon work supported by the National Aeronautics and Space Administration under Contract NNM10AA11C issued through the New Frontiers Program, and by Contracts 80NSSC18K0239 (for JLM) and 80NSSC18K0229 (for RDH) issued through the OSIRIS-REx Participating Scientist Program. The work of SRC was conducted at the Jet Propulsion Laboratory, California Institute of Technology under a contract with the National Aeronautics and Space Administration. COMSOL, the software used to perform the modeling, is commercially available (https://www.comsol.com/), and the NAIF SPICE Toolkit is publicly available (https://naif.jpl.nasa.gov/naif/toolkit.html). All parameters needed to reproduce our simulations are described in the text. The raw numbers for all figures in the text (excluding Figures 1 and 4) and the strain energy density profiles needed to produce Figures 5 to 8 can be obtained from the Earth and Space Science Open Archive (doi.org/10.1002/essoar.10501385.2).

Author Contributions

Per the CRediT (Contributor Roles Taxonomy) system:
Conceptualization: J.L.M., R.D.H., C.W.Ha., R.-L.B., S.R.S., W.F.B., K.J.W., H.J.C., D.S.L
Data Curation:
Formal analysis: J.L.M., C.W.He., S.R.C.
Funding acquisition: J.L.M., D.S.L, K.J.W.
Investigation: J.L.M., C.W.He. , S.R.C.
Methodology: J.L.M.
Resources:
Software:
Validation: J.L.M.
Visualization: J.L.M.
Writing – original draft: J.L.M.
Writing – review & editing: J.L.M., C.W.He. , S.R.C., R.D.H., C.W.Ha., R.-L.B., S.R.S., W.F.B., K.J.W., H.J.C., D.S.L.